

Theory of spin excitations in a quantum spin-nematic state

Andrew Smerald and Nic Shannon

Okinawa Institute of Science and Technology, Onna-son, Okinawa 904-0412, Japan

and H. H. Wills Physics Laboratory, University of Bristol, Tyndall Av, BS8-ITL, United Kingdom

(Received 18 July 2013; revised manuscript received 28 October 2013; published 27 November 2013)

The idea that a quantum magnet could act like a liquid crystal, breaking spin-rotation symmetry without breaking time-reversal symmetry, holds an abiding fascination. However, the very fact that spin nematic states do not break time-reversal symmetry renders them “invisible” to the most common probes of magnetism—they do *not* exhibit magnetic Bragg peaks, a static splitting of lines in NMR spectra, or oscillations in μ SR. Nonetheless, as a consequence of breaking spin-rotation symmetry, spin-nematic states *do* possess a characteristic spectrum of dispersing excitations which *could* be observed in experiment. With this in mind, we develop a symmetry-based description of long-wavelength excitations in a spin-nematic state, based on an SU(3) generalization of the quantum nonlinear σ model. We use this field theory to make explicit predictions for inelastic neutron scattering, and argue that the wavelike excitations it predicts could be used to identify the symmetries broken by the otherwise unseen spin-nematic order.

DOI: [10.1103/PhysRevB.88.184430](https://doi.org/10.1103/PhysRevB.88.184430)

PACS number(s): 75.10.Jm, 75.40.Gb

I. INTRODUCTION

The search for quantum spin liquids, magnets which do not order at *any* temperature, has become one of the cause célèbre of modern physics.¹ Another equally intriguing possibility is that the spins of a quantum magnet *do* order, but in a way which does not transform like a spin. Such a state would be almost invisible to the usual probes of magnetism, and could therefore appear as a “hidden order.” A concrete example of this is the quantum spin-nematic—a magnetic analog of a liquid crystal.^{2–8}

Conventional nematic order is associated with the directional order of rod- or disklike molecules. Spin-nematic order occurs where the *fluctuations* of a spin mimic a uniaxial molecule, selecting an axis without selecting a direction along it. For example, a system could exhibit fluctuations such that $\langle (S^x)^2 \rangle = \langle (S^y)^2 \rangle \neq \langle (S^z)^2 \rangle$ while maintaining $\langle \mathbf{S} \rangle = 0$. Such a phase would break spin-rotation symmetry *without* breaking time-reversal symmetry. This particular type of spin-nematic state can be described as “ferroquadrupolar” (FQ), since the fluctuations form a quadrupole moment of \mathbf{S} with a common axis on all sites (for an introduction, see Ref. 9). More generally, quadrupole moments tend to select orthogonal axes. Examples of this kind of “antiferroquadrupolar” (AFQ) order are shown in Figs. 1–3.

There are now good theoretical reasons to believe that spin-nematic order should occur in a range of low-dimensional and frustrated systems. However, because the spin-nematic state does not break time-reversal symmetry, it is “invisible” to the tests commonly used to discern magnetic order, namely the existence of magnetic Bragg peaks in elastic neutron scattering, the splitting of lines in NMR spectra, or through the asymmetry of oscillations in μ SR spectra. Nevertheless, since excitations of the spin-nematic state induce a fluctuating dipole moment, spin-nematic order can, in principle, be detected by *dynamic* probes of magnetism, such as inelastic neutron scattering or the NMR $1/T_1$ relaxation rate. This hints at an interesting question—if we can not measure the symmetry breaking in a spin-nematic state directly, can we infer it from the associated excitations?

In this paper, we set aside all questions of the microscopic origin of spin-nematic order, and attempt to say something about what the excitations of a spin-nematic state would look like, assuming it existed. To this end, we develop a phenomenological, symmetry-based description of long-wavelength excitations in AFQ spin-nematic states, based on an SU(3) generalization of the quantum nonlinear σ model, and use it to make concrete predictions for inelastic neutron scattering and the dynamical quadrupolar susceptibility.

We build on a long history of studying spin-nematic states. In one dimension, theoretical studies support the existence of Luttinger liquids with dominant power-law correlations of spin-quadrupole moments (and in some cases, higher-order spin-multipoles), in frustrated ferromagnetic spin chains,^{10–23} in spin-1/2 ladders with cyclic exchange^{24,25} and for spin-1 models with biquadratic interactions.^{26–28}

In two dimensions, theoretical studies suggest the existence of a bond-centred, spin-nematic ground state in models of spin-1/2 frustrated ferromagnets on the square^{29–33} (see Fig. 3) and the triangular lattices,^{34,35} and of a generalized chiral nematic phase on the square lattice.^{6,36} Similarly, two-dimensional, spin-1 models with biquadratic interactions support $T = 0$ nematic order.^{5,37–45} Entropy-driven nematic order has also been widely studied in the context of the classical Heisenberg model on the kagome lattice.^{46,47}

In three dimensions, quantum Monte Carlo calculations find evidence for a spin-1 nematic state in the bilinear-biquadratic model,⁴⁵ and classical spin-nematic states have been proposed on various frustrated lattices.^{46–51} Weakly coupled chains in magnetic field also exhibit long-range spin-nematic order.⁵²

Recently, the study of spin-nematic order has been re-energized by the proposal that it might occur in a number of real materials. The unusual magnetic ground state of the spin-1 layered magnetic insulator NiGa₂S₄⁵³ has been discussed in terms of both FQ^{39,54} and AFQ^{40,41} order (cf. Fig. 1), and spin-freezing in the presence of FQ correlations,⁵⁵ with the bilinear-biquadratic model on a triangular lattice used as a prototype for calculations. Exact diagonalization studies of the relevant multiple spin-exchange model suggest that the “spin liquid” ground state of thin films of ³He might

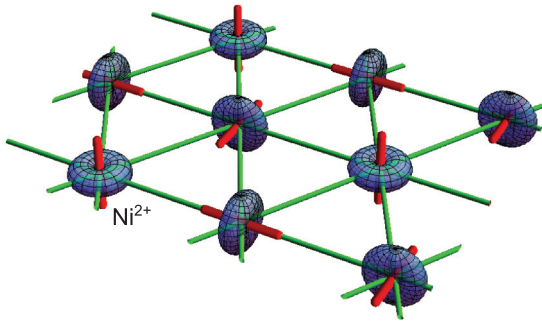


FIG. 1. (Color online) Three-sublattice antiferroquadrupolar (AFQ) spin-nematic state, found in the spin-1 bilinear-biquadratic model on a triangular lattice, and studied in the context of NiGa_2As_2 .^{39–41} The probability distribution of spin fluctuations (shown as a blue surface) define orthogonal directions on neighboring sites. The directors describing this AFQ state are represented by red cylinders.

be associated with a three-sublattice, bond-centred, AFQ phase^{34,35} (cf. Fig. 2). Related calculations suggest that a two-sublattice, bond-centred, AFQ spin-nematic state (cf. Fig. 3) might also be realized in the spin-1/2 frustrated Heisenberg model relevant to a family of square lattice vanadates.²⁹ Finally, magnetization measurements on the spin-chain system LiCuVO_4 show a phase transition close to saturation, which has been interpreted as the onset of a bond-centred, AFQ state.^{56,57}

In parallel with this new work on magnetic insulators, there has been an explosion of interest in electronic-nematic states in itinerant transition-metal compounds, and a resurgence of interest in the study of multipolar hidden-order phases in rare-earth materials.⁵⁸ Since these systems are typically metallic and/or subject to strong spin-orbit coupling, somewhat different considerations apply, and we will not attempt to review either subject here. We concentrate instead on local moments with a high degree of spin-rotational symmetry.

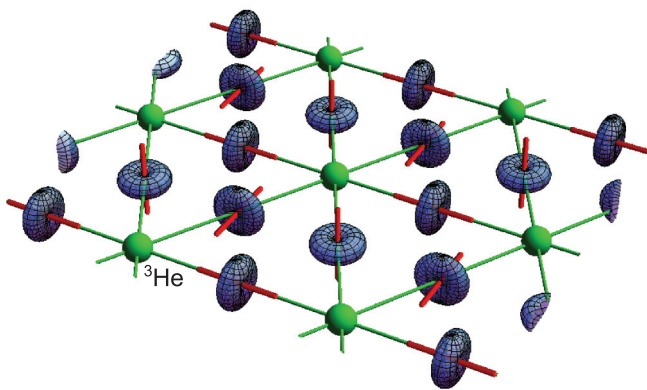


FIG. 2. (Color online) The three-sublattice, bond-centred, antiferroquadrupolar (AFQ) spin-nematic state proposed to exist in thin films of ^3He .^{34,35} This system can be modelled using a multiple spin exchange model of ^3He atoms with nuclear spin-1/2 (represented by green spheres), on a two-dimensional triangular lattice. For a range of parameters bordering on ferromagnetism, the ground state of this model is a three-sublattice AFQ order in which spin fluctuations (shown as a blue surface) are orthogonal on neighboring bonds. The directors describing this AFQ state are represented by red cylinders.

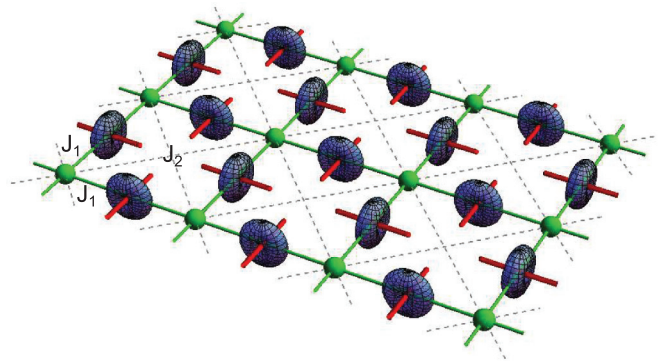


FIG. 3. (Color online) Two-sublattice, bond-centred, antiferroquadrupolar (AFQ) spin-nematic state found bordering the ferromagnetic state in both the spin-1/2 $J_1 - J_2$ Heisenberg model and the spin-1/2 multiple spin exchange model on the square lattice.^{29–33} Magnetic ions are denoted by green spheres, and the probability distribution of spin fluctuations on each bond is shown as a blue surface. The directors describing this AFQ state are represented by red cylinders.

While this brings some simplifications, the microscopic models needed to describe thin films of ^3He (see Ref. 35) and LiCuVO_4 (see Refs. 21 and 57) are already very complex, with dominant nearest-neighbor ferromagnetic interactions frustrated by a large number of competing antiferromagnetic exchange pathways. The complexity of these models points to the need for a phenomenological description of AFQ order, which makes explicit the physical nature of its excitations, and parameterizes them in terms of the smallest possible number of experimentally measurable parameters.

In this article, we develop a symmetry-based description of the long-wavelength excitations of three-sublattice AFQ order on the triangular lattice. Our approach, based on an $\text{SU}(3)$ generalization of the quantum nonlinear σ model, could be applied equally to the spin-1 magnet NiGaS_2 (see Refs. 39–41), or to thin films of ^3He (see Refs. 34 and 35). With minor modifications, the action we derive also offers a description of the two-sublattice AFQ order proposed to occur in LiCuVO_4 (see Refs. 21 and 57), and square lattice frustrated ferromagnets.²⁹ In fact, it can be modified to describe any system where spin-quadrupoles display short- or long-range, noncollinear order. The only requirement is that the Hamiltonian either has a continuous symmetry [e.g., $\text{SU}(2)$ or $\text{U}(1)$], or is close to having a continuous symmetry.

In order to demonstrate the validity of this approach, we show explicitly how our σ -model like action can be derived from a microscopic model exhibiting three-sublattice AFQ order, the spin-1 bilinear-biquadratic (BBQ) model on a triangular lattice.^{39–41} At long wavelength, the resulting continuum theory exactly reproduces published results for “flavor wave” analysis of the lattice model.^{39,41} However, the continuum theory is both independent of the “flavor wave” theory and far more general, and could equally well be parametrized from experiment, or from analysis of a more-complicated microscopic model where the “flavor wave” approach is not applicable.

Good reviews exist of “flavor wave” techniques for spin-nematic order,⁹ but σ -model approaches have yet to be

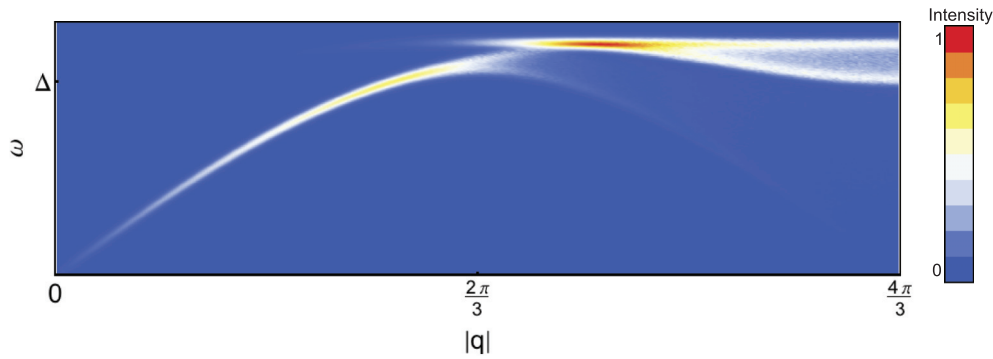


FIG. 4. (Color online) Prediction for inelastic neutron-scattering from a powder sample of a triangular-lattice magnet with a three-sublattice antiferroquadrupolar (AFQ) spin-nematic ground state. Spectral weight is found predominantly in the upper, spin-wave band, but vanishes approaching $\mathbf{q} = 0$. Intensity in the lower, quadrupole-wave band is weaker and vanishes approaching the magnetic ordering vector $|\mathbf{q}| = 4\pi/3$. Results are taken from the linear “flavor wave” analysis of the spin-1 bilinear-biquadratic model [see Eq. (1)], as described in Ref. 40 and Sec. II of this paper, for parameters $J_1 = 1$, $J_2 = 1.22$. The prediction for the dynamic structure factor $S(\mathbf{q}, \omega)$ has been integrated over angle and convoluted with a Gaussian of FWHM $\omega = 0.042\Delta$, where $\Delta = 6\sqrt{J_2(J_1 - J_2)}$.

reviewed, and have so far been restricted to FQ order.^{59–62} We therefore provide a complete and pedagogical account of the steps needed to derive a nonlinear σ -model description of AFQ order.

The fact that different branches of excitation correspond to different rotations of the order parameter, allows us to assign each branch of excitations a clear physical meaning. In the case of three-sublattice AFQ order, we identify two, physically-distinct types of magnetic excitation—three degenerate branches of “quadrupole waves,” the gapless, linearly-dispersing Goldstone modes of AFQ order, and three degenerate branches of gapped, high-energy “spin-wave” excitations. The spin-wave excitations have a substantial fluctuating dipole moment, and so should be clearly visible in experiment.

Having constructed a general theory for the long-wavelength excitations of the three-sublattice AFQ spin-nematic states, we are in position to make explicit predictions for inelastic neutron scattering experiments. An example is given in Fig. 4. Observation of these features in experiment would provide strong evidence for spin-nematic order, and a means of distinguishing between different types of spin-nematic states. We also show predictions for the dynamic quadrupole susceptibility. This may be measurable using, for example, resonant x-ray scattering.

When calculating the experimental response we neglect interaction between the modes. Since we are primarily interested in the universal, long wavelength features, it is expected that this is a good approximation. We will return to the role of interactions in a future publication.⁶³ We note that any treatment of the two-particle continuum excitations *must* take the role of three- and four-particle interactions into account if it is to obey the symmetry-constrained sum rules, and for this reason we do not discuss the continuum in this publication.

The remainder of this article is structured as follows. In Sec. II, we develop a theory of long-wavelength excitations in a three-sublattice AFQ spin-nematic state. In Sec. III, we explore how the excitations of each of these states would manifest themselves in inelastic neutron scattering experiments. In Sec. IV, we consider the dynamical quadrupolar susceptibility.

Finally, in Sec. V, we conclude with a summary of results and discussion of their experimental context. Readers who are already expert in σ models, or simply uninterested in these technical details, are invited to pass directly to Sec. III, where all key results are summarized. Results for spin-nematic states in two-sublattice states, in applied magnetic field and predictions for the NMR $1/T_1$ relaxation rate, will be presented in a separate publication.⁶³

II. CONTINUUM THEORY OF THREE-SUBLATTICE AFQ ORDER

A. Minimal microscopic model

To keep our continuum theory grounded in microscopic reality, it is helpful to be able to derive it directly from a concrete lattice model, even though the resulting field theory will have far broader applicability. The simplest microscopic model with an AFQ ground state is the spin-1 bilinear-biquadratic (BBQ) model on a triangular lattice.^{2,5,39} This model is defined by

$$\mathcal{H}_{\Delta}^{\text{BBQ}} = \sum_{\langle ij \rangle} J_1 \mathbf{S}_i \cdot \mathbf{S}_j + J_2 (\mathbf{S}_i \cdot \mathbf{S}_j)^2, \quad (1)$$

where the sum on $\langle ij \rangle$ runs over the nearest-neighbour bonds of a triangular lattice.

The mean-field phase diagram for the spin-1 BBQ model on a triangular lattice,^{9,39} reproduced in Fig. 5, exhibits an extended region of three-sublattice AFQ order for $J_2 > 0$, terminating in a point for $J_1 = J_2$ where the symmetry of the model is enlarged from $SU(2)$ to $SU(3)$.⁵ AFQ order is accompanied by a ferroquadrupolar (FQ) phase for $J_2 < 0$. Conventional ferromagnetic (FM) and three-sublattice “120°” antiferromagnetic (AFM) phases separate these two spin-nematic states. A very similar phase diagram is found in exact diagonalization,³⁹ and the existence of AFQ and FQ phases for closely related BBQ models has been independently confirmed by density matrix renormalization group calculations,⁶⁶ and quantum Monte Carlo simulations.⁴⁵

For $J_2 > J_1 > 0$, $\mathcal{H}_{\Delta}^{\text{BBQ}}$ [see Eq. (1)] favors states in which the quadrupole moments on neighboring sites take on

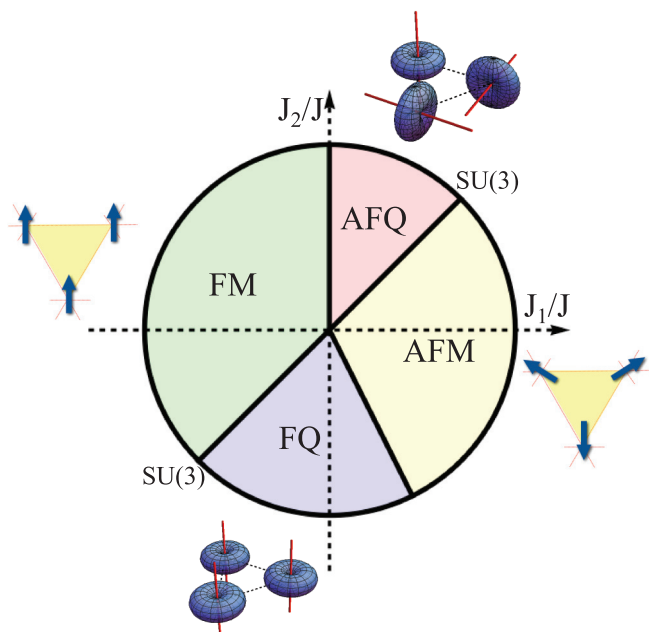


FIG. 5. (Color online) The mean-field, ground-state phase diagram for the spin-1 bilinear-biquadratic (BBQ) model on a triangular lattice $\mathcal{H}_{\Delta}^{\text{BBQ}}$ [see Eq. (1)], following Refs. 9 and 39, showing two distinct regions of spin-nematic order. In the ferro-quadrupolar (FQ) phase, all directors are aligned. In the three-sublattice antiferroquadrupolar (AFQ) phase, directors on different sublattices are orthogonal. The model also supports two conventional magnetic phases—the ferromagnet (FM); and the three-sublattice “120°” antiferromagnet (AFM). For $J_1 = J_2$, the symmetry of the model is increased from SU(2) to SU(3).

perpendicular directions. The relative simplicity of this model follows from the fact that each spin-1 can form a quadrupole by itself, and the triangular lattice is tripartite, and so naturally supports a three-sublattice state in which all quadrupoles are orthogonal to one another. The fact that an approximate ground-state wave function can be written in a site-factorized form⁹ makes it possible to calculate physically interesting quantities perturbatively from the Hamiltonian using “flavor wave” theory^{5,37–41,67–69}—the SU(3) generalization of the more usual SU(2) spin-wave theory.

The “flavor wave” approach does not generalize easily to the complicated spin-1/2 models that are relevant to systems such as ³He and LiCuVO₄. However, it provides an important benchmark for the field-theoretical approach developed in this article. In what follows we briefly review some of the features of the spin-1 BBQ model on a triangular lattice, including a useful mean-field parametrization in terms of spin coherent states, which makes explicit the director nature of the order parameter.^{9,39,59}

Following Refs. 39–41, the Hamiltonian (1) can be rewritten in the form

$$\begin{aligned} \mathcal{H}_{\Delta}^{\text{BBQ}} = & \sum_{\langle ij \rangle} \left(J_1 - \frac{J_2}{2} \right) \mathbf{S}_i \cdot \mathbf{S}_j \\ & + \frac{J_2}{2} \mathbf{Q}_i \cdot \mathbf{Q}_j + \frac{J_2}{3} S^2 (S+1)^2, \end{aligned} \quad (2)$$

where the quadrupole operator \mathbf{Q} is given by

$$\mathbf{Q} = \begin{pmatrix} Q^{x^2-y^2} \\ Q^{3z^2-r^2} \\ Q^{xy} \\ Q^{yz} \\ Q^{xz} \end{pmatrix} = \begin{pmatrix} (S^x)^2 - (S^y)^2 \\ \frac{1}{\sqrt{3}} [2(S^z)^2 - (S^x)^2 - (S^y)^2] \\ S^x S^y + S^y S^x \\ S^y S^z + S^z S^y \\ S^x S^z + S^z S^x \end{pmatrix}. \quad (3)$$

The operator \mathbf{Q} encodes the five linearly independent degrees of freedom contained in the traceless, symmetric tensor,

$$Q^{\alpha\beta} = -\frac{2}{3} S(S+1) \delta^{\alpha\beta} + S^{\alpha} S^{\beta} + S^{\beta} S^{\alpha}. \quad (4)$$

It is common practice to parametrize the two magnetic exchange interactions as

$$J_1 = \bar{J} \cos \theta, \quad J_2 = \bar{J} \sin \theta, \quad (5)$$

and to plot phase diagrams on a circle, as in Fig. 5. In this article, we concentrate on the AFQ phase, bounded by the SU(3) point at $\theta = \pi/4$.

Since spin-nematic states are time-reversal invariant, it is useful to introduce a set of basis states that respect this symmetry. Following,^{5,9,59} we consider the following linear superpositions of the usual spin-1 basis states,

$$|x\rangle = i \frac{|1\rangle - |\bar{1}\rangle}{\sqrt{2}}, \quad |y\rangle = \frac{|1\rangle + |\bar{1}\rangle}{\sqrt{2}}, \quad |z\rangle = -i|0\rangle. \quad (6)$$

A general wave function for a spin-1 spin at a site j can then be written in the form

$$|\mathbf{d}_j\rangle = d_j^x |x\rangle + d_j^y |y\rangle + d_j^z |z\rangle, \quad (7)$$

where $\mathbf{d}_j = (d_j^x, d_j^y, d_j^z)$ is a 3-vector of complex numbers. It is sometimes convenient to write this out explicitly in real and imaginary components as

$$\mathbf{d}_j = \mathbf{u}_j + i \mathbf{v}_j. \quad (8)$$

Requiring the wave function to be normalized gives the constraint

$$\mathbf{d}_j \cdot \bar{\mathbf{d}}_j = 1 \quad \text{or} \quad \mathbf{u}_j^2 + \mathbf{v}_j^2 = 1, \quad (9)$$

while the overall phase is set by the equation

$$\mathbf{d}_j^2 = \bar{\mathbf{d}}_j^2 \quad \text{or} \quad \mathbf{u}_j \cdot \mathbf{v}_j = 0. \quad (10)$$

Since the phase does not affect any physical observables, one is free to choose this convenient value. As a consequence of Eqs. (9) and (10), there are four degrees of freedom associated with each site.

Within the spin-coherent state framework, the operator products appearing in the Hamiltonian (2) can be calculated as

$$\mathbf{S}_i \cdot \mathbf{S}_j = |\mathbf{d}_i \cdot \bar{\mathbf{d}}_j|^2 - |\mathbf{d}_i \cdot \mathbf{d}_j|^2, \quad (11)$$

$$\mathbf{Q}_i \cdot \mathbf{Q}_j = |\mathbf{d}_i \cdot \bar{\mathbf{d}}_j|^2 + |\mathbf{d}_i \cdot \mathbf{d}_j|^2 - \frac{2}{3},$$

where the spin value has been set to spin-1. As a result, the Hamiltonian is

$$\mathcal{H}_{\Delta}^{\text{BBQ}} = \sum_{\langle ij \rangle} J_1 |\mathbf{d}_i \cdot \bar{\mathbf{d}}_j|^2 + (J_2 - J_1) |\mathbf{d}_i \cdot \mathbf{d}_j|^2 + J_2. \quad (12)$$

By minimizing this equation, a mean-field, low-temperature phase diagram can be mapped out, as shown in Fig. 5.

Purely real or purely imaginary values of \mathbf{d} correspond to static nematic states, in which the quadrupole operators take on finite expectation values, but the spin-dipole operators do not. The associated director is parallel to the “director vector;” \mathbf{d} . When \mathbf{d} has both real and imaginary components, this corresponds to mixing in a nonzero, static dipole moment, given within the coherent state representation by

$$\mathbf{S}_j = 2\mathbf{u}_j \times \mathbf{v}_j. \quad (13)$$

$$\begin{pmatrix} S^x \\ S^y \\ S^z \\ Q^{x^2-y^2} \\ Q^{3z^2-r^2} \\ Q^{xy} \\ Q^{yz} \\ Q^{xz} \end{pmatrix} = \begin{pmatrix} id^z\bar{d}^y - id^y\bar{d}^z \\ id^z\bar{d}^x - id^x\bar{d}^z \\ id^x\bar{d}^y - id^y\bar{d}^x \\ |d^y|^2 - |d^x|^2 \\ \frac{1}{\sqrt{3}}(|d^x|^2 + |d^y|^2 - 2|d^z|^2) \\ d^x\bar{d}^y + d^y\bar{d}^x \\ d^y\bar{d}^z + d^z\bar{d}^y \\ -d^x\bar{d}^z - d^z\bar{d}^x \end{pmatrix} = \begin{pmatrix} 2(u^y v^z - v^y u^z) \\ 2(u^z v^x - v^z u^x) \\ 2(u^x v^y - v^x u^y) \\ (u^y)^2 + (v^y)^2 - (u^x)^2 - (v^x)^2 \\ \frac{1}{\sqrt{3}}[(u^x)^2 + (v^x)^2 + (u^y)^2 + (v^y)^2 - 2(u^z)^2 - 2(v^z)^2] \\ 2(u^x u^y + v^x v^y) \\ 2(u^y u^z + v^y v^z) \\ -2(u^x u^z + v^x v^z) \end{pmatrix}. \quad (14)$$

B. Continuum theory at the SU(3) point

1. Why start here?

For $J_1 = J_2$, the symmetry of the spin-1 BBQ model $\mathcal{H}_\Delta^{\text{BBQ}}$ [see Eq. (1)] is enlarged from SU(2) to SU(3). Exactly at this point, the ground states of $\mathcal{H}_\Delta^{\text{BBQ}}$ include both the three-sublattice AFQ state *and* the three-sublattice “120°” Néel antiferromagnet. Moreover, generic three-sublattice ground states can be constructed from both dipole and quadrupole moments of spins. These physically distinct building blocks are connected by SU(3) rotations that transform \mathbf{S} into \mathbf{Q} —and vice versa—as well as rotating one spin (or quadrupole) configuration into another. These SU(3) rotations are precisely what is needed to describe the long-wavelength excitations of spin-nematic order, and the SU(3) point ($J_1 = J_2$) therefore provides a very natural starting point for building a continuum theory of three-sublattice AFQ order.

In the remainder of Sec. II B below, we construct a σ model description of long-wavelength excitations of three-sublattice AFQ order at the SU(3) point. We arrive at a field theory comprising of six identical, linearly dispersing Goldstone modes, associated with rotations of a triad of \mathbf{d} vectors. Then, in Sec. II D, we explore the consequence of those terms in the Hamiltonian which break this SU(3) symmetry down to the more generic SU(2), introducing these as perturbations about the SU(3) point. This leads to a completely general theory of long-wavelength excitations in a three-sublattice AFQ state, comprising three gapless Goldstone modes and three gapped spin-wave excitations.

The structure of this field theory is completely determined by the symmetries of the order parameter, and therefore independent of its derivation. However, starting from the SU(3) point of the spin-1 BBQ model allows us to achieve a controlled derivation of a field theory for a three-sublattice AFQ state from a microscopic model, in a way which keeps the physical nature of its excitations in view. This approach draws inspiration from earlier work on FQ order

The largest dipole moment occurs when \mathbf{u} and \mathbf{v} are equal in magnitude (although even in this state there remain quadrupole operators with nonzero expectation values).

The physical observables in the system are expectation values of the dipole and quadrupole operators, \mathbf{S} and \mathbf{Q} . It is useful to write these in the coherent state representation, terms of the vectors \mathbf{d} , \mathbf{u} , and \mathbf{v} , as

in one dimension,^{59–61} and for the three-sublattice 120° AFM state on the triangular lattice.^{70,71} In order to keep the text accessible and reasonably self-contained, the necessary steps are described in some detail below.

2. Brief summary of calculation

Before embarking on the calculation, it is useful to briefly summarize the main steps. We start with a single triangular plaquette, which hosts a triad of orthogonal director vectors, and define matrices that describe all the physically relevant, infinitesimal rotations of this triad in the complex vector space of \mathbf{d} (i.e., those spanning the coset SU(3)/H, where H defines the isotropy subgroup). By the successive action of these matrices, *any* physical configuration of the three directors can be accessed. Some of these matrices perform global rotations of the director triad, within its complex vector space, and therefore leave the energy invariant. The remainder perform local rotations of the director configuration and thus change the energy of the configuration [see Figs. 6 and 7]. In analogy with the collinear antiferromagnet,^{72,73} which undergoes a local ferromagnetic canting, these matrices can be described as a “canting” of the orthogonal director configuration.

The triangular plaquette acts as the basic unit from which to build the triangular lattice (see Fig. 8). By defining fields at the center of plaquettes, it is possible to move from a lattice theory written in terms of a Hamiltonian to a continuum theory in terms of a Lagrangian. The fields inherit the properties of the rotation matrices. As in the case of the collinear antiferromagnet,^{72,73} in moving from the lattice Hamiltonian to the continuum Lagrangian, it is necessary to introduce a dynamical term, which arises from the quantum mechanical overlap of director configurations.

Since we wish to describe the low-temperature excitations of the antiferroquadrupolar state, it is reasonable to assume that the directors are approximately orthogonal to one another on short length scales. In consequence, the Lagrangian can be

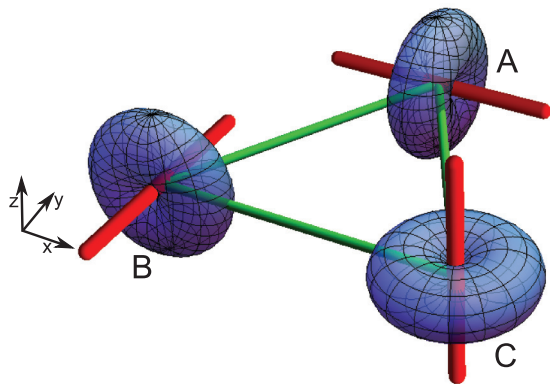


FIG. 6. (Color online) The basic building-block of three-sublattice antiferroquadrupolar (AFQ) order—a triangular plaquette with directors (red cylinders) orientated as described in Eq. (16). These directors describe the spontaneous breaking of spin-rotation symmetry in the AFQ phase and are orthogonal on each of the three sublattices. The probability of a spin fluctuation vanishes parallel to the directors and is maximal in the plane perpendicular to them—the associated probability distribution is shown as a blue surface.

expanded in terms of the ‘canting’ fields. These can then be eliminated by a Gaussian integral, and the resulting action is an $SU(3)$ symmetric nonlinear σ model.

One way to gain a better physical understanding of the resulting theory is to linearize the fields. This allows a natural division of the modes into those with predominantly quadrupole-fluctuation character and those with spin-fluctuation character. This forms the starting point for calculations of the experimental signatures that could prove the existence of nematic order (see Sec. III).

3. Structure of the ground-state manifold

The order parameter for the AFQ phase of $\mathcal{H}_{\Delta}^{\text{BBQ}}$ [see Eq. (1)] can be defined on a triangular plaquette containing a triad of directors [cf. Fig. 6]. These directors, which we will label A, B, and C, could, in principle, be located on the sites

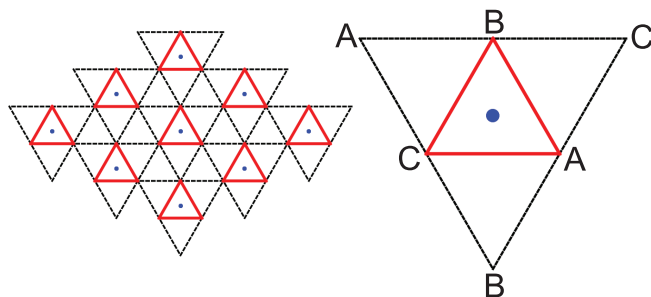


FIG. 8. (Color online) The partitioning of the triangular lattice used in the derivation of the field theory for the three-sublattice antiferroquadrupolar (AFQ) spin-nematic state. The lattice is split into clusters containing three sites and nine bonds, such that each cluster retains the point group symmetries of the lattice. Fields are defined at the center of the clusters (blue dots), and the fact that the directors are associated with the vertices of the lattice is built into the continuum theory by a gradient expansion about this point.

of the lattice, as is the case here, or on the bonds, as is the case in multiple spin exchange models relevant to thin films of ^3He .

At the high-symmetry $SU(3)$ point, $J_1 = J_2 = J$, the Hamiltonian, $\mathcal{H}_{\Delta}^{\text{BBQ}}$ [see Eq. (12)], simplifies to

$$\mathcal{H}_{SU(3)} = J(|\mathbf{d}_A \cdot \bar{\mathbf{d}}_B|^2 + |\mathbf{d}_B \cdot \bar{\mathbf{d}}_C|^2 + |\mathbf{d}_C \cdot \bar{\mathbf{d}}_A|^2) + 3J. \quad (15)$$

This can be minimized by requiring $\mathbf{d}_i \cdot \bar{\mathbf{d}}_j = 0$ on every bond, resulting in a three-sublattice order in which neighboring \mathbf{d} vectors are orthogonal. There is no requirement that \mathbf{d} should be real (or imaginary) and therefore the ground-state manifold includes both quadrupolar, dipolar, and mixed phases.

One choice for the ground state of such a system is

$$\mathbf{d}_A^{\text{gs}} = (1, 0, 0), \quad \mathbf{d}_B^{\text{gs}} = (0, 1, 0), \quad \mathbf{d}_C^{\text{gs}} = (0, 0, 1). \quad (16)$$

This corresponds to an AFQ state in which the three directors lie along the principle axes, (x, y, z) , and is illustrated in Fig. 6.

The Hamiltonian (15) is invariant under the global rotation $\mathbf{d} \rightarrow \mathbf{U}\mathbf{d}$, provided that $\mathbf{U}^{-1} = \mathbf{U}^\dagger$, making clear the $SU(3)$

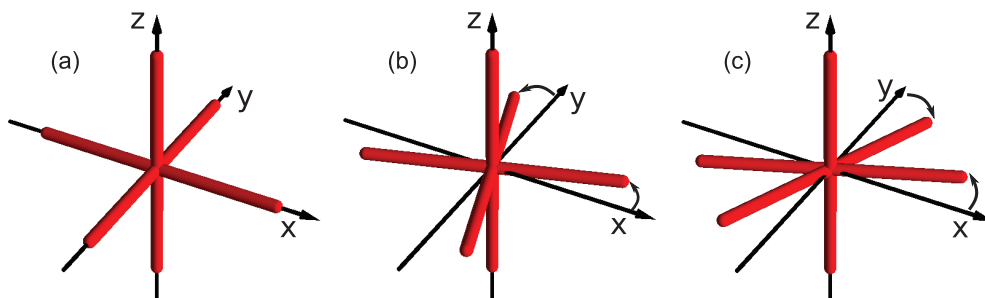


FIG. 7. (Color online) Real component of the complex director configurations for antiferroquadrupolar (AFQ) order on a triangular plaquette [see Fig. 6], showing the action of global rotations $\mathbf{U}(\phi)$ and local rotations associated with the canting fields \mathbf{l} . Directors (red cylinders) on the three sites of the plaquette are combined at the plaquette center. (a) The orthogonal ground state given in Eq. (16). (b) The result of acting on this particular ground state with $\mathbf{D}_{\Delta}(\phi_1, 0, \dots)$ [see Eq. (20)]. This performs a global rotation of the directors around the z axis, and a different orthogonal ground state is generated. (c) The result of acting with $\mathbf{D}_{\Delta}(0, \dots, l_1^z, 0, \dots)$, which is seen to rotate directors orientated along the x and y axes in opposite directions around the z axis. In consequence, the angle between the directors changes, and this costs energy according to the Hamiltonian $\langle \mathcal{H}_{\Delta}^{\text{BBQ}} \rangle$ [see Eq. (12)].

symmetry of the ground state. However, not all of the ground states generated by these rotations are physically distinct, since one is free to fix the phase on a site. There are, in fact, six distinct generators of rotations that transform the system between inequivalent ground states. These are conveniently represented using six of the eight Gell-Mann matrices:

$$\begin{aligned}\lambda_1 &= \begin{pmatrix} 0 & -i & 0 \\ i & 0 & 0 \\ 0 & 0 & 0 \end{pmatrix}, & \lambda_2 &= \begin{pmatrix} 0 & 0 & -i \\ 0 & 0 & 0 \\ i & 0 & 0 \end{pmatrix}, \\ \lambda_3 &= \begin{pmatrix} 0 & 0 & 0 \\ 0 & 0 & -i \\ 0 & i & 0 \end{pmatrix}, & \lambda_4 &= \begin{pmatrix} 0 & 1 & 0 \\ 1 & 0 & 0 \\ 0 & 0 & 0 \end{pmatrix}, & (17) \\ \lambda_5 &= \begin{pmatrix} 0 & 0 & 1 \\ 0 & 0 & 0 \\ 1 & 0 & 0 \end{pmatrix}, & \lambda_6 &= \begin{pmatrix} 0 & 0 & 0 \\ 0 & 0 & 1 \\ 0 & 1 & 0 \end{pmatrix}.\end{aligned}$$

The other two Gell-Mann matrices are diagonal and are not physically relevant, as they change the phase of the directors.

Starting from a particular ground state of the triangular plaquette, such as the one described in Eq. (16), the global rotation matrix

$$\mathbf{U}(\boldsymbol{\phi}) = \exp\left(i \sum_{p=1}^6 \lambda_p \phi_p\right), \quad (18)$$

can be used to explore all other possible ground-state configurations, where $\boldsymbol{\phi} = (\phi_1, \dots, \phi_6)$. This matrix acts globally on all three \mathbf{d} vectors, and thus preserves the angle between them in the complex vector space. In consequence, these rotations have a zero energy cost, and a real space illustration of this is shown in Fig. 7(b).

The global rotations of the order parameter can be split into two categories. In order to see this, it is useful to use the shorthand notation $\mathbf{U}_1 = \mathbf{U}(\phi_1, 0, 0, 0, 0, 0)$ and similarly for $\mathbf{U}_2, \dots, \mathbf{U}_6$. The matrices $\mathbf{U}_1, \mathbf{U}_2$, and \mathbf{U}_3 perform rotations of the directors that are real in the sense that, if \mathbf{d} is real [as in Eq. (16)], it will remain so under these transformations. Applied to the AFQ ground state, they act only to rotate the quadrupole moments. However, the matrices $\mathbf{U}_4, \mathbf{U}_5$, and \mathbf{U}_6 transform a real \mathbf{d} vector into a complex one in such a way as to mix a dipolar component into the AFQ ground state. We will return to this point below when classifying spin excitations.

C. Canting of a plaquette

Our ultimate aim is to describe the long-wavelength, director-wave fluctuations about the “invisible” AFQ spinematic ground state—the “waves in the unseen.” This involves canting of the director triad out of the orthogonal ground state.

A necessary first step is to construct a matrix \mathbf{D}_Δ that can be used to access any configuration of three \mathbf{d} vectors on a triangular plaquette. In order to do this, it is useful to introduce

a second set of generators:

$$\begin{aligned}\mu_1 &= \begin{pmatrix} 0 & -i & 0 \\ -i & 0 & 0 \\ 0 & 0 & 0 \end{pmatrix}, & \mu_2 &= \begin{pmatrix} 0 & 0 & -i \\ 0 & 0 & 0 \\ -i & 0 & 0 \end{pmatrix}, \\ \mu_3 &= \begin{pmatrix} 0 & 0 & 0 \\ 0 & 0 & -i \\ 0 & -i & 0 \end{pmatrix}, & \mu_4 &= \begin{pmatrix} 0 & 1 & 0 \\ -1 & 0 & 0 \\ 0 & 0 & 0 \end{pmatrix}, & (19) \\ \mu_5 &= \begin{pmatrix} 0 & 0 & -1 \\ 0 & 0 & 0 \\ 1 & 0 & 0 \end{pmatrix}, & \mu_6 &= \begin{pmatrix} 0 & 0 & 0 \\ 0 & 0 & 1 \\ 0 & -1 & 0 \end{pmatrix}.\end{aligned}$$

When these act on a triad of \mathbf{d} vectors [see Fig. 7(a)], they change the angles between the vectors, thus changing the energy, according to Eq. (15) [see Fig. 7(c)]. Any configuration of the three \mathbf{d} vectors can be accessed from Eq. (16) using

$$\begin{aligned}\mathbf{D}_\Delta(\boldsymbol{\phi}, \mathbf{l}) &= \exp\left(i \sum_{p=1}^6 \lambda_p \phi_p + i \mu_1 l_1^z + i \mu_2 l_1^y + i \mu_3 l_1^x \right. \\ &\quad \left. + i \mu_4 l_2^z + i \mu_5 l_2^y + i \mu_6 l_2^x\right), & (20)\end{aligned}$$

where the vector \mathbf{l} is defined by

$$\mathbf{l} = \begin{pmatrix} l^z \\ l^x \\ l^y \end{pmatrix} = \begin{pmatrix} l_1^z + i l_2^z \\ l_1^x + i l_2^x \\ l_1^y + i l_2^y \end{pmatrix}. \quad (21)$$

This notation may appear unnatural at first sight but will prove convenient for calculation. A completely general configuration of the three \mathbf{d} vectors is thus given by

$$\mathbf{d}_A = \mathbf{D}_\Delta \cdot \begin{pmatrix} 1 \\ 0 \\ 0 \end{pmatrix}, \quad \mathbf{d}_B = \mathbf{D}_\Delta \cdot \begin{pmatrix} 0 \\ 1 \\ 0 \end{pmatrix}, \quad \mathbf{d}_C = \mathbf{D}_\Delta \cdot \begin{pmatrix} 0 \\ 0 \\ 1 \end{pmatrix}. \quad (22)$$

We now make the assumption that the system has at least short-range order, and thus expand for small canting fields \mathbf{l} . Retaining fields up to $\mathcal{O}(\mathbf{l})$,

$$\mathbf{d}_A = \mathbf{U} \cdot \begin{pmatrix} 1 \\ \bar{l}^z \\ l^y \end{pmatrix}, \quad \mathbf{d}_B = \mathbf{U} \cdot \begin{pmatrix} l^z \\ 1 \\ \bar{l}^x \end{pmatrix}, \quad \mathbf{d}_C = \mathbf{U} \cdot \begin{pmatrix} \bar{l}^y \\ l^x \\ 1 \end{pmatrix}, \quad (23)$$

and it follows that the length and phase constraints of Eqs. (9) and (10) hold to $\mathcal{O}(l^2)$.

The eventual aim is to eliminate the canting fields \mathbf{l} from the partition function by integration. What will remain is a theory describing the dynamics of the order parameter matrix \mathbf{U} in terms of the variables $\boldsymbol{\phi}$.

1. Continuum limit

We now consider how to pass from a lattice theory to a continuum theory of the AFQ state. The lattice can be partitioned into clusters based on triangular plaquettes (as shown in Fig. 8). The director fields are defined at the center of these clusters, and the physical location of the directors

is taken into account by performing a gradient expansion. The continuum limit involves the assumption that physically interesting variation takes place on a length scale much larger than the lattice constant a and so gradients within the plaquette are small.

One of the requirements of a continuum field theory is that it should describe the dynamics of both the broken symmetry state *and* the nearby paramagnetic region, in which the order parameter is assumed to be locally robust but slowly varying over macroscopic length scales. It is therefore necessary to allow the fields to fluctuate in space and time,

$$\begin{aligned} \mathbf{d}_A(\mathbf{r}, \tau) &= \mathbf{U}(\mathbf{r}, \tau) \begin{pmatrix} 1 \\ \bar{l}^Z(\mathbf{r}, \tau) \\ l^Y(\mathbf{r}, \tau) \end{pmatrix} + \mathcal{O}(l^2), \\ \mathbf{d}_B(\mathbf{r}, \tau) &= \mathbf{U}(\mathbf{r}, \tau) \begin{pmatrix} l^Z(\mathbf{r}, \tau) \\ 1 \\ \bar{l}^X(\mathbf{r}, \tau) \end{pmatrix} + \mathcal{O}(l^2), \\ \mathbf{d}_C(\mathbf{r}, \tau) &= \mathbf{U}(\mathbf{r}, \tau) \begin{pmatrix} \bar{l}^Y(\mathbf{r}, \tau) \\ l^X(\mathbf{r}, \tau) \\ 1 \end{pmatrix} + \mathcal{O}(l^2). \end{aligned} \quad (24)$$

A useful parametrization of the matrix \mathbf{U} is

$$\mathbf{U}(\mathbf{r}, \tau) = \begin{pmatrix} n_A^X(\mathbf{r}, \tau) & n_B^X(\mathbf{r}, \tau) & n_C^X(\mathbf{r}, \tau) \\ n_A^Y(\mathbf{r}, \tau) & n_B^Y(\mathbf{r}, \tau) & n_C^Y(\mathbf{r}, \tau) \\ n_A^Z(\mathbf{r}, \tau) & n_B^Z(\mathbf{r}, \tau) & n_C^Z(\mathbf{r}, \tau) \end{pmatrix}, \quad (25)$$

where the complex fields $\mathbf{n}_i(\mathbf{r}, \tau)$, with $i = \{A, B, C\}$, inherit the length and phase constraints of the \mathbf{d} vectors [see Eqs. (9) and (10)],

$$\mathbf{n}_i \cdot \bar{\mathbf{n}}_i = 1, \quad \mathbf{n}_i^2 - \bar{\mathbf{n}}_i^2 = 0, \quad (26)$$

and are also required to be orthogonal to one another according to

$$\mathbf{n}_i \cdot \bar{\mathbf{n}}_j = 0, \quad i \neq j. \quad (27)$$

The apparent 18 degrees of freedom of the \mathbf{n}_i fields is reduced to six by the 12 constraints, as expected. The reason that the parametrization in terms of $\mathbf{n}_i(\mathbf{r}, \tau)$ is useful is that these fields are mutually orthogonal, of unit length, and of fixed phase, and can therefore be interpreted as a ground-state director configuration. In consequence, there are two equivalent formulations of the field theory: in terms of the rotation matrix $\mathbf{U}(\mathbf{r}, \tau)$; or in terms of the fields $\mathbf{n}_i(\mathbf{r}, \tau)$. We will make use of both in what follows.

Differentiating the constraints, Eqs. (26) and (27), leads to the relations

$$\begin{aligned} \mathbf{n}_i \cdot \partial_\lambda \bar{\mathbf{n}}_i &= -\bar{\mathbf{n}}_i \cdot \partial_\lambda \mathbf{n}_i, & \mathbf{n}_i \cdot \partial_\lambda \mathbf{n}_i &= \bar{\mathbf{n}}_i \cdot \partial_\lambda \bar{\mathbf{n}}_i, \\ \mathbf{n}_i \cdot \partial_\lambda \bar{\mathbf{n}}_j &= -\bar{\mathbf{n}}_j \cdot \partial_\lambda \mathbf{n}_i, & i &\neq j, \end{aligned} \quad (28)$$

where the partial derivative ∂_λ can be with respect to any space-time variable. These relations prove very useful for simplifying subsequent expressions.

The partition function can be written in terms of a functional integral over all director configurations,

$$\mathcal{Z}_\Delta^{\text{SU}(3)} = \int \mathcal{D}[\mathbf{d}] e^{-\mathcal{S}_\Delta^{\text{SU}(3)}[\mathbf{d}]}, \quad (29)$$

where $\mathcal{S}_\Delta^{\text{SU}(3)}[\mathbf{d}]$ is the Euclidean action and the integration measure $\mathcal{D}[\mathbf{d}]$ includes the δ function constraints on the length and phase of the director. The action can be split into Hamiltonian and kinetic terms,

$$\mathcal{S}_\Delta^{\text{SU}(3)} = \mathcal{S}_{\text{kin}} + \mathcal{S}_{\mathcal{H}[\text{SU}(3)]}, \quad (30)$$

where \mathcal{S}_{kin} is a dynamic, geometric-phase term and $\mathcal{S}_{\mathcal{H}[\text{SU}(3)]}$ accounts for the energy cost of static director configurations at the SU(3) point.

2. The Hamiltonian term

The energy cost of a particular static configuration of directors is given by Eq. (12). In principle, the Hamiltonian term in the action, $\mathcal{S}_{\mathcal{H}}$, takes into account all static configurations of directors. However, we make the approximation that only those with a slow spatial variation are important.

The Hamiltonian term is given by

$$\begin{aligned} \mathcal{S}_{\mathcal{H}[\text{SU}(3)]} &= \int_0^\beta d\tau \mathcal{H}_{\text{SU}(3)} \\ &= \frac{2}{3\sqrt{3}a^2} \int_0^\beta d\tau \int d^2r \mathcal{H}_{\text{SU}(3), \text{clus}}, \end{aligned} \quad (31)$$

where $\mathcal{H}_{\text{SU}(3), \text{clus}}$ refers to the Hamiltonian for a single cluster, and the numerical prefactor is related to the area of the cluster.

The gradient expansion of the fields in terms of the small parameter a is given by

$$\begin{aligned} \mathbf{d}_j(\mathbf{r} + \boldsymbol{\epsilon}_i, \tau) &= \mathbf{d}_j(\mathbf{r}, \tau) + a(\boldsymbol{\epsilon}_i \cdot \nabla) \mathbf{d}_j(\mathbf{r}, \tau) \\ &\quad + \frac{a^2}{2!} (\boldsymbol{\epsilon}_i \cdot \nabla)^2 \mathbf{d}_j(\mathbf{r}, \tau) + \mathcal{O}(a^3), \end{aligned} \quad (32)$$

where $\boldsymbol{\epsilon}_i$ is the vector connecting the center of the cluster to the lattice sites within it (cf. Fig. 8).

Expanding the Hamiltonian to second order in the lattice parameter a gives

$$\begin{aligned} \mathcal{H}_{\text{SU}(3), \text{clus}} &\approx 3J(|\bar{\mathbf{d}}_A(\mathbf{r}, \tau) \cdot \mathbf{d}_B(\mathbf{r}, \tau)|^2 + |\bar{\mathbf{d}}_B(\mathbf{r}, \tau) \cdot \mathbf{d}_C(\mathbf{r}, \tau)|^2 \\ &\quad + |\bar{\mathbf{d}}_C(\mathbf{r}, \tau) \cdot \mathbf{d}_A(\mathbf{r}, \tau)|^2) + \frac{3Ja^2}{2} \\ &\quad \times \sum_{\lambda=X,Y} [|\bar{\mathbf{d}}_A \cdot \partial_\lambda \mathbf{d}_B|^2 + |\bar{\mathbf{d}}_B \cdot \partial_\lambda \mathbf{d}_C|^2 \\ &\quad + |\bar{\mathbf{d}}_C \cdot \partial_\lambda \mathbf{d}_A|^2]. \end{aligned} \quad (33)$$

The first term in this expression vanishes if the system is an AFQ ground state. Fluctuations about this can be expanded in terms of the canting field \mathbf{l} using

$$\begin{aligned} \bar{\mathbf{d}}_A(\mathbf{r}, \tau) \cdot \mathbf{d}_B(\mathbf{r}, \tau) &\approx 2l^Z(\mathbf{r}, \tau), \\ \bar{\mathbf{d}}_B(\mathbf{r}, \tau) \cdot \mathbf{d}_C(\mathbf{r}, \tau) &\approx 2l^X(\mathbf{r}, \tau), \\ \bar{\mathbf{d}}_C(\mathbf{r}, \tau) \cdot \mathbf{d}_A(\mathbf{r}, \tau) &\approx 2l^Y(\mathbf{r}, \tau). \end{aligned} \quad (34)$$

Since the gradient terms are already $\mathcal{O}(a^2)$, the fields $\mathbf{d}(\mathbf{r}, \tau)$ can be replaced by the orthogonal fields $\mathbf{n}(\mathbf{r}, \tau)$, giving the Hamiltonian

$$\begin{aligned} \mathcal{H}_{\text{SU}(3), \text{clus}} &\approx 12J\mathbf{l} \cdot \bar{\mathbf{l}} + \frac{3Ja^2}{2} \sum_{\lambda=X,Y} (|\bar{\mathbf{n}}_A \cdot \partial_\lambda \mathbf{n}_B|^2 \\ &\quad + |\bar{\mathbf{n}}_B \cdot \partial_\lambda \mathbf{n}_C|^2 + |\bar{\mathbf{n}}_C \cdot \partial_\lambda \mathbf{n}_A|^2). \end{aligned} \quad (35)$$

3. The kinetic term

The action describing long wave-length fluctuations of the AFQ state also contains a kinetic energy term. This is quantum-mechanical in origin, and a consequence of the overcompleteness of the coherent states used to represent spin configurations. At a semiclassical level, it describes the rotational motion of the directors, and can therefore be interpreted as a geometrical phase. For a more detailed explanation, we refer the interested reader to the chapters on spin path integrals in Refs. 72 and 73.

The contribution of the kinetic term to the action is

$$S_{\text{kin}} \approx \int_0^\beta d\tau \frac{2}{3\sqrt{3}a^2} \int d^2r \sum_i \bar{\mathbf{d}}_i \cdot \partial_\tau \mathbf{d}_i, \quad (36)$$

where spatial gradient terms have been ignored. To first order in the canting field \mathbf{l} ,

$$\sum_i \bar{\mathbf{d}}_i \cdot \partial_\tau \mathbf{d}_i \approx \text{Tr}[\mathbf{U}^\dagger \cdot \partial_\tau \mathbf{U}] + 2(\mathbf{s} \cdot \mathbf{l} - \bar{\mathbf{s}} \cdot \bar{\mathbf{l}}), \quad (37)$$

where the complex field $\mathbf{s}(\mathbf{r}, \tau)$ is defined as

$$\mathbf{s} = \begin{pmatrix} (\mathbf{U}^\dagger \cdot \partial_\tau \mathbf{U})_{21} \\ (\mathbf{U}^\dagger \cdot \partial_\tau \mathbf{U})_{32} \\ (\mathbf{U}^\dagger \cdot \partial_\tau \mathbf{U})_{13} \end{pmatrix} = \begin{pmatrix} \bar{\mathbf{n}}_B \cdot \partial_\tau \mathbf{n}_A \\ \bar{\mathbf{n}}_C \cdot \partial_\tau \mathbf{n}_B \\ \bar{\mathbf{n}}_A \cdot \partial_\tau \mathbf{n}_C \end{pmatrix}. \quad (38)$$

The kinetic term gives an imaginary contribution to the Euclidean Lagrangian. Derivatives of the field \mathbf{l} vanish, since they are total derivatives and can therefore be converted to a vanishing surface integral.

4. Integrating out fluctuations

Having derived an action for long-wavelength fluctuations of the AFQ state, the task that remains is to eliminate the canting fields $\mathbf{l}(\mathbf{r}, \tau)$, so as to arrive at an action written entirely in terms of the order parameter $\mathbf{n}(\mathbf{r}, \tau)$. Taking into account both potential and kinetic energy terms in the Hamiltonian, we start from the partition function

$$\mathcal{Z}_\Delta^{\text{SU}(3)} \propto \int \prod_{i \neq j} \mathcal{D}\mathbf{n}_i \mathcal{D}\bar{\mathbf{n}}_i \mathcal{D}\mathbf{l} \mathcal{D}\bar{\mathbf{l}} \delta(\mathbf{n}_i \cdot \bar{\mathbf{n}}_i - 1) \delta(\mathbf{n}_i^2 - \bar{\mathbf{n}}_i^2) \times \delta(\mathbf{n}_i \cdot \bar{\mathbf{n}}_j) e^{-\mathcal{S}_\Delta^{\text{SU}(3)}[\mathbf{n}_A, \bar{\mathbf{n}}_A, \mathbf{n}_B, \bar{\mathbf{n}}_B, \mathbf{n}_C, \bar{\mathbf{n}}_C, \mathbf{l}, \bar{\mathbf{l}}]}, \quad (39)$$

where the action

$$\mathcal{S}_\Delta^{\text{SU}(3)}[\mathbf{n}_A, \bar{\mathbf{n}}_A, \mathbf{n}_B, \bar{\mathbf{n}}_B, \mathbf{n}_C, \bar{\mathbf{n}}_C, \mathbf{l}, \bar{\mathbf{l}}] = \int_0^\beta d\tau \frac{2}{3\sqrt{3}a^2} \int d^2r \mathcal{L}_\Delta^{\text{SU}(3)} \quad (40)$$

is written in terms of the Lagrangian

$$\mathcal{L}_\Delta^{\text{SU}(3)} \approx \text{Tr}[\mathbf{U}^\dagger \cdot \partial_\tau \mathbf{U}] + 2(\mathbf{s} \cdot \mathbf{l} - \bar{\mathbf{s}} \cdot \bar{\mathbf{l}}) + 12J\mathbf{l} \cdot \bar{\mathbf{l}} + \frac{3Ja^2}{2} \sum_{\lambda=x,y} (|\bar{\mathbf{n}}_A \cdot \partial_\lambda \mathbf{n}_B|^2 + |\bar{\mathbf{n}}_B \cdot \partial_\lambda \mathbf{n}_C|^2 + |\bar{\mathbf{n}}_C \cdot \partial_\lambda \mathbf{n}_A|^2). \quad (41)$$

The canting fields \mathbf{l} and $\bar{\mathbf{l}}$ enter the Lagrangian at a quadratic level and can therefore be eliminated via a Gaussian integral, or, equivalently, using the steepest-descent approximation.

This process is slightly simpler if the two fields are decoupled by the linear transformation

$$\mathbf{l} = \mathbf{l}_1 + i\mathbf{l}_2, \quad \bar{\mathbf{l}} = \mathbf{l}_1 - i\mathbf{l}_2, \quad (42)$$

where \mathbf{l}_1 and \mathbf{l}_2 are real. Taking functional derivatives with respect to these fields gives

$$\frac{\delta \mathcal{L}_\Delta^{\text{SU}(3)}}{\delta \mathbf{l}_1} \approx 2(\mathbf{s} - \bar{\mathbf{s}}) + 24J\mathbf{l}_1 \approx 0, \quad (43)$$

$$\frac{\delta \mathcal{L}_\Delta^{\text{SU}(3)}}{\delta \mathbf{l}_2} \approx 2i(\mathbf{s} + \bar{\mathbf{s}}) + 24J\mathbf{l}_2 \approx 0,$$

and these equations are resolved as

$$\mathbf{l}_1 \approx -\frac{1}{12J}(\mathbf{s} - \bar{\mathbf{s}}), \quad \mathbf{l}_2 \approx -\frac{i}{12J}(\mathbf{s} + \bar{\mathbf{s}}). \quad (44)$$

At this point, it is helpful to introduce a ‘‘director stiffness’’

$$\rho_d = Ja^2, \quad (45)$$

describing the energy cost of twisting the order parameter, and the generalized susceptibility

$$\chi_\perp = \frac{2}{9J}, \quad (46)$$

associated with fluctuations of the canting field \mathbf{l} .

Substituting the canting fields, Eq. (44), into the Lagrangian, Eq. (41), and using Eqs. (38) and (25) to re-express this in terms of the fields \mathbf{n}_i , we arrive at

$$\mathcal{S}_\Delta^{\text{SU}(3)}[\mathbf{n}_A, \bar{\mathbf{n}}_A, \mathbf{n}_B, \bar{\mathbf{n}}_B, \mathbf{n}_C, \bar{\mathbf{n}}_C] = \frac{1}{\sqrt{3}a^2} \int_0^\beta d\tau \int d^2r \left[\frac{2}{3} \sum_i \bar{\mathbf{n}}_i \cdot \partial_\tau \mathbf{n}_i + \chi_\perp (|\bar{\mathbf{n}}_A \cdot \partial_\tau \mathbf{n}_B|^2 + |\bar{\mathbf{n}}_B \cdot \partial_\tau \mathbf{n}_C|^2 + |\bar{\mathbf{n}}_C \cdot \partial_\tau \mathbf{n}_A|^2) + \rho_d \sum_{\lambda=x,y} (|\bar{\mathbf{n}}_A \cdot \partial_\lambda \mathbf{n}_B|^2 + |\bar{\mathbf{n}}_B \cdot \partial_\lambda \mathbf{n}_C|^2 + |\bar{\mathbf{n}}_C \cdot \partial_\lambda \mathbf{n}_A|^2) \right], \quad (47)$$

with associated partition function

$$\mathcal{Z}_\Delta^{\text{SU}(3)} \propto \int \prod_{i \neq j} \mathcal{D}\mathbf{n}_i \mathcal{D}\bar{\mathbf{n}}_i \delta(\mathbf{n}_i \cdot \bar{\mathbf{n}}_i - 1) \delta(\mathbf{n}_i^2 - \bar{\mathbf{n}}_i^2) \times \delta(\mathbf{n}_i \cdot \bar{\mathbf{n}}_j) e^{-\mathcal{S}_\Delta^{\text{SU}(3)}[\mathbf{n}_A, \bar{\mathbf{n}}_A, \mathbf{n}_B, \bar{\mathbf{n}}_B, \mathbf{n}_C, \bar{\mathbf{n}}_C]}, \quad (48)$$

where the canting fields have been eliminated at a Gaussian level.

Equivalently, Eq. (25) can be used to write the action, Eq. (47), in terms of the unitary matrices $\mathbf{U}(\mathbf{r}, \tau)$ as

$$\mathcal{S}_\Delta^{\text{SU}(3)}[\mathbf{U}] = \frac{1}{2\sqrt{3}a^2} \int_0^\beta d\tau \int d^2r \left\{ \frac{4}{3} \text{Tr}[\mathbf{U}^\dagger \cdot \partial_\tau \mathbf{U}] + \chi_\perp [\text{Tr}(\partial_\tau \mathbf{U}^\dagger \cdot \partial_\tau \mathbf{U}) - \sum_m |[\mathbf{U}^\dagger \cdot \partial_\tau \mathbf{U}]_{mm}|^2] + \rho_d \sum_{\lambda=x,y} [\text{Tr}(\partial_\lambda \mathbf{U}^\dagger \cdot \partial_\lambda \mathbf{U}) - \sum_m |[\mathbf{U}^\dagger \cdot \partial_\lambda \mathbf{U}]_{mm}|^2] \right\}, \quad (49)$$

where $m = \{1, 2, 3\}$ labels matrix elements. This formulation of the action is further removed from the physical state than Eq. (47) but makes explicit the SU(3) symmetry of the Hamiltonian.

5. Linearizing the order parameter fields

The physical nature of the excitations of the AFQ state—and, in particular, the division into quadrupole-wave and spin-wave modes—is easier to understand once the action describing them has been linearized. This can be achieved by expanding fluctuations about the AFQ ground state to leading order in ϕ . We will consider in detail the interaction of the ϕ fields in a future publication.⁶³

After linearization, the unitary matrix field $\mathbf{U}(\mathbf{r}, \tau)$ [see Eq. (18)] is approximated by

$$\mathbf{U}(\mathbf{r}, \tau) \approx \begin{pmatrix} 1 & \phi_1 + i\phi_4 & -\phi_2 + i\phi_5 \\ -\phi_1 + i\phi_4 & 1 & \phi_3 + i\phi_6 \\ \phi_2 + i\phi_5 & -\phi_3 + i\phi_6 & 1 \end{pmatrix}, \quad (50)$$

where the angular variables $\phi_p = \phi_p(\mathbf{r}, \tau)$ fluctuate in both space and time. It follows from Eq. (25) that the fields $\mathbf{n}_i(\mathbf{r}, \tau)$ are given by

$$\begin{aligned} \mathbf{n}_A(\mathbf{r}, \tau) &\approx \begin{pmatrix} 1 \\ -\phi_1 + i\phi_4 \\ \phi_2 + i\phi_5 \end{pmatrix}, \\ \mathbf{n}_B(\mathbf{r}, \tau) &\approx \begin{pmatrix} \phi_1 + i\phi_4 \\ 1 \\ -\phi_3 + i\phi_6 \end{pmatrix}, \\ \mathbf{n}_C(\mathbf{r}, \tau) &\approx \begin{pmatrix} -\phi_2 + i\phi_5 \\ \phi_3 + i\phi_6 \\ 1 \end{pmatrix}, \end{aligned} \quad (51)$$

making explicit that the fields $\phi_p(\mathbf{r}, \tau)$ have a simple interpretation in terms of small, local angles of rotation away from the direction of spontaneous symmetry breaking.

Equation (14) can now be used to reconstruct the fluctuating dipolar and quadrupolar moments on each sublattice. To leading order in $\phi_p(\mathbf{r}, \tau)$, these can be written as

$$\mathbf{S}_A \approx 2 \begin{pmatrix} 0 \\ -\phi_5 \\ \phi_4 \end{pmatrix}, \quad \mathbf{S}_B \approx 2 \begin{pmatrix} \phi_6 \\ 0 \\ -\phi_4 \end{pmatrix}, \quad \mathbf{S}_C \approx 2 \begin{pmatrix} -\phi_6 \\ \phi_5 \\ 0 \end{pmatrix}, \quad (52)$$

and

$$\mathbf{Q}_A \approx \begin{pmatrix} -1 \\ 1/\sqrt{3} \\ -2\phi_1 \\ 0 \\ -2\phi_2 \end{pmatrix}, \quad \mathbf{Q}_B \approx \begin{pmatrix} 1 \\ 1/\sqrt{3} \\ 2\phi_1 \\ -2\phi_3 \\ 0 \end{pmatrix}, \quad \mathbf{Q}_C \approx \begin{pmatrix} 0 \\ -2/\sqrt{3} \\ 0 \\ 2\phi_3 \\ 2\phi_2 \end{pmatrix}. \quad (53)$$

This shows that the fields ϕ_1 , ϕ_2 , and ϕ_3 are primarily associated with fluctuations of the quadrupole moments, and so justifies the name “quadrupole waves.” Since the fields ϕ_4 , ϕ_5 , and ϕ_6 are primarily associated with *transverse* fluctuations of the dipole moments, we refer to them as “spin waves.”

In Sec. IID, we extend this analysis to also include time derivatives of the ϕ fields. References 64 and 65 contain animations showing the nature of the quadrupole-wave⁶⁴ and spin-wave⁶⁴ modes that follow from Eq. (53).

Linearizing the action $\mathcal{S}_\Delta^{\text{SU}(3)}[\mathbf{U}]$ [see Eq. (49)] also enables us to eliminate the δ function constraints from the partition function $\mathcal{Z}_\Delta^{\text{SU}(3)}$ [see Eq. (48)], to give

$$\mathcal{Z}_\Delta^{\text{SU}(3)} \propto \int \mathcal{D}\phi e^{-\mathcal{S}_\Delta^{\text{SU}(3)}[\phi]}, \quad (54)$$

where the linearized action is

$$\begin{aligned} \mathcal{S}_\Delta^{\text{SU}(3)}[\phi] &\approx \frac{1}{\sqrt{3}a^2} \int_0^\beta d\tau \int d^2r \\ &\times \sum_{p=1}^6 \left[\chi_\perp (\partial_\tau \phi_p)^2 + \rho_d \sum_{\lambda=x,y} (\partial_\lambda \phi_p)^2 \right]. \end{aligned} \quad (55)$$

At this level of approximation, the equations of motion for each field are independent of one another and given by

$$(\chi_\perp \partial_\tau^2 + \rho_d \partial_x^2 + \rho_d \partial_y^2) \phi_p = 0. \quad (56)$$

These can be solved by the ansatz

$$\phi_p = A_p e^{i\mathbf{q}\cdot\mathbf{r} + \omega_q \tau}, \quad (57)$$

and in consequence, the dispersion (shown in Fig. 9) is

$$\omega_q = \sqrt{\frac{\rho_d}{\chi_\perp}} |\mathbf{q}| = v |\mathbf{q}|, \quad (58)$$

with the director-wave velocity,

$$v = \sqrt{\frac{\rho_d}{\chi_\perp}} = \frac{3Ja}{\sqrt{2}}. \quad (59)$$

Here, the vector \mathbf{q} measures the distance in reciprocal space from the center of the magnetic Brillouin zone (mbz), which is centered on the K point, $\mathbf{k}_K = (4\pi/3, 0)$, as shown in Fig. 10.

Thus, at the SU(3) point, there are six gapless excitations, which disperse linearly with the same velocity, regardless of whether they have spin-wave or quadrupole-wave character. This reflects the large ground-state manifold at the SU(3) point, which consists of all three-sublattice orthogonal arrangements of the \mathbf{d} vectors, and therefore includes both the AFQ and AFM states [cf. Fig. 5]. In Sec. IID, we show that, as J_2 is increased and dipolar order becomes energetically unfavorable, only three linearly dispersing modes remain—the quadrupole-wave modes, which are the Goldstone modes of AFQ order.

We note that Tsunetsugu and Arikawa^{40,41} have previously determined the dispersion of Eq. (1) in the AFQ phase using a linearized “flavor wave” theory. At the high-symmetry SU(3) point, they find

$$\omega_{\mathbf{k}} = 3J\sqrt{1 - |\gamma_{\mathbf{k}}|^2}, \quad (60)$$

where

$$\gamma_{\mathbf{k}} = \frac{1}{3} \left(e^{ik_x a} + 2e^{\frac{-ik_x a}{2}} \cos \frac{\sqrt{3}k_y a}{2} \right). \quad (61)$$

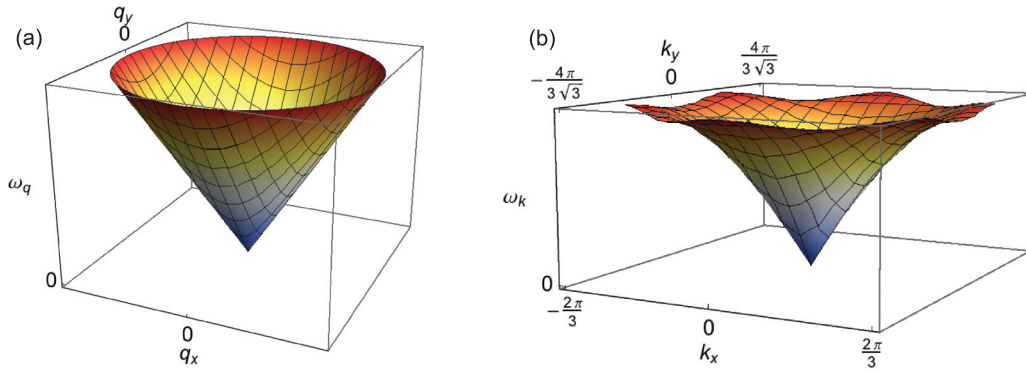


FIG. 9. (Color online) The dispersion of magnetic excitations at the SU(3) point. (a) Prediction of the continuum field theory $\mathcal{S}_{\Delta}^{\text{SU}(3)}$ [see Eq. (55)]. (b) Prediction of the spin-1 bilinear-biquadratic (BBQ) model on a triangular lattice, $\mathcal{H}_{\Delta}^{\text{BBQ}}$ [see Eq. (1)] for $J_1 = J_2$. Approaching the ordering vector $\mathbf{k} = \mathbf{k}_M$ ($\mathbf{q} = 0$), the continuum theory and the lattice theory match exactly. At this high-symmetry point, there is a sixfold degenerate branch of linearly dispersive, gapless excitations. These can be split into three modes that primarily describe fluctuations of quadrupole moments (quadrupole waves) and three that primarily describe fluctuations of dynamically generated dipole moments (spin waves). These three spin-wave fields become gapped on entering the antiferroquadrupolar (AFQ) phase bordering the SU(3) point.

As $\mathbf{k} \rightarrow 0$, the limiting value of Eq. (60) is $\omega_{\mathbf{k}} \approx v|\mathbf{k}|$, where the velocity $v = 3Ja/\sqrt{2}$ is identical to the one predicted by the field theory [see Eq. (59)].

D. Continuum theory away from the SU(3) point

1. Symmetry breaking terms

The SU(3) point of $\mathcal{H}_{\Delta}^{\text{BBQ}}$ [see Eq. (1)], $J_2 = J_1 = J$, has an artificially high symmetry. For $J_2 > J_1$, the symmetry of $\mathcal{H}_{\Delta}^{\text{BBQ}}$ is reduced to SU(2), with important implications for the excitations of the AFQ state. In what follows, we construct a continuum field theory for the AFQ phase by perturbing away from the SU(3) point. The most significant change, required for the stability of AFQ order, is the opening of a gap to the three spin-wave modes.

Following the notation of Sec. II B, the Hamiltonian $\mathcal{H}_{\Delta}^{\text{BBQ}}$ [see Eq. (1)] can be written

$$\mathcal{H}_{\text{BBQ}} = \mathcal{H}_{\text{SU}(3)} + \Delta\mathcal{H}_{\text{SU}(2)}, \quad (62)$$

where

$$\Delta\mathcal{H}_{\text{SU}(2)} = (J_2 - J_1) \sum_{\langle ij \rangle} |\mathbf{d}_i \cdot \mathbf{d}_j|^2, \quad (63)$$

and $\mathcal{H}_{\text{SU}(3)}$ is defined by Eq. (15). In order to develop a perturbative expansion around the high-symmetry SU(3) point, we make the assumption that $J_2 - J_1 \ll J_1, J_2$. This assumption breaks down for $\theta \rightarrow \pi/2$, and places a limit on the range of wavelengths for which the σ -model description developed in this Section is a valid description of $\mathcal{H}_{\Delta}^{\text{BBQ}}$ [see Eq. (1)].

The kinetic term in the action \mathcal{S}_{kin} [see Eq. (31)] is unchanged since it is a property of the coherent state representation of the spin states, not of the Hamiltonian. The change to the Hamiltonian term in the action $\mathcal{S}_{\mathcal{H}}$ for a three-sublattice AFQ state can be calculated by performing a gradient expansion for the 3-site, nine-bond cluster shown in Fig. 8, following the example of Eq. (32). This gives

$$\begin{aligned} \Delta\mathcal{H}_{\text{SU}(2), \text{clus}} \approx & 3(J_2 - J_1)[|\mathbf{d}_A(\mathbf{r}, \tau) \cdot \mathbf{d}_B(\mathbf{r}, \tau)|^2 + |\mathbf{d}_B(\mathbf{r}, \tau) \cdot \mathbf{d}_C(\mathbf{r}, \tau)|^2 + |\mathbf{d}_C(\mathbf{r}, \tau) \cdot \mathbf{d}_A(\mathbf{r}, \tau)|^2] + \frac{3(J_2 - J_1)a^2}{2} \sum_{\lambda=x,y} (|\mathbf{d}_A \cdot \partial_{\lambda} \mathbf{d}_B|^2 \\ & + |\mathbf{d}_B \cdot \partial_{\lambda} \mathbf{d}_C|^2 + |\mathbf{d}_C \cdot \partial_{\lambda} \mathbf{d}_A|^2) - \frac{3(J_2 - J_1)a^2}{4} \sum_{\lambda=x,y} [(\mathbf{d}_A \cdot \mathbf{d}_B)(\partial_{\lambda} \bar{\mathbf{d}}_A \cdot \partial_{\lambda} \bar{\mathbf{d}}_B) + (\bar{\mathbf{d}}_A \cdot \bar{\mathbf{d}}_B)(\partial_{\lambda} \mathbf{d}_A \cdot \partial_{\lambda} \mathbf{d}_B) \\ & + (\mathbf{d}_B \cdot \mathbf{d}_C)(\partial_{\lambda} \bar{\mathbf{d}}_B \cdot \partial_{\lambda} \bar{\mathbf{d}}_C) + (\bar{\mathbf{d}}_B \cdot \bar{\mathbf{d}}_C)(\partial_{\lambda} \mathbf{d}_B \cdot \partial_{\lambda} \mathbf{d}_C) + (\mathbf{d}_C \cdot \mathbf{d}_A)(\partial_{\lambda} \bar{\mathbf{d}}_C \cdot \partial_{\lambda} \bar{\mathbf{d}}_A) + (\bar{\mathbf{d}}_C \cdot \bar{\mathbf{d}}_A)(\partial_{\lambda} \mathbf{d}_C \cdot \partial_{\lambda} \mathbf{d}_A)], \end{aligned} \quad (64)$$

where the expansion has been truncated at second order in a .

Consider the product

$$\mathbf{d}_A(\mathbf{r}, \tau) \cdot \mathbf{d}_B(\mathbf{r}, \tau) \approx (1, \bar{l}^z, l^y) \cdot \mathbf{U}^T \mathbf{U} \cdot \begin{pmatrix} l^z \\ 1 \\ \bar{l}^x \end{pmatrix}, \quad (65)$$

where the matrices can be expressed as

$$\mathbf{U}^T \mathbf{U} = \begin{pmatrix} \mathbf{n}_A^2 & \mathbf{n}_A \cdot \mathbf{n}_B & \mathbf{n}_C \cdot \mathbf{n}_A \\ \mathbf{n}_A \cdot \mathbf{n}_B & \mathbf{n}_B^2 & \mathbf{n}_B \cdot \mathbf{n}_C \\ \mathbf{n}_C \cdot \mathbf{n}_A & \mathbf{n}_B \cdot \mathbf{n}_C & \mathbf{n}_C^2 \end{pmatrix}. \quad (66)$$

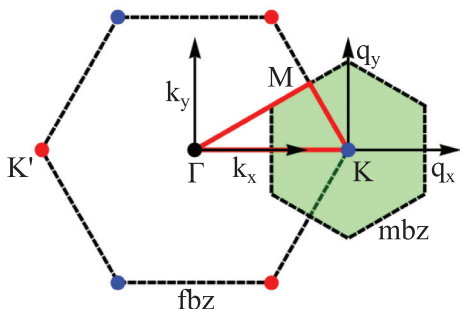


FIG. 10. (Color online) The full Brillouin zone (fbz) of the triangular lattice, together with the reduced magnetic Brillouin zone (mbz) for three-sublattice order. Important symmetry points are labeled Γ [$\mathbf{k}_\Gamma = (0,0)$], M [$\mathbf{k}_M = (\pi/3, \pi/\sqrt{3})$], K [$\mathbf{k}_K = (4\pi/3, 0)$], and K' [$\mathbf{k}_{-K} = -\mathbf{k}_K$]. In the field theory for the three-sublattice antiferroquadrupolar (AFQ) state, the Γ and K' points are folded onto the K point, and the wave vector \mathbf{q} measures the deviation from this point. The circuit in reciprocal space Γ - K - M - Γ followed when plotting the inelastic neutron scattering intensity in Fig. 12 is indicated in red.

The ground state of the system involves purely real (or purely imaginary) \mathbf{d} vectors, and therefore at low T , it is reasonable to approximate

$$\mathbf{n}_i^2 \approx 1 \quad (67)$$

and

$$\mathbf{n}_i \cdot \mathbf{n}_j \ll 1, \quad i \neq j. \quad (68)$$

It follows that

$$\mathbf{n}_i \cdot \mathbf{n}_j \approx -\bar{\mathbf{n}}_i \cdot \bar{\mathbf{n}}_j \quad (69)$$

and therefore

$$\begin{aligned} \mathbf{d}_A(\mathbf{r}, \tau) \cdot \mathbf{d}_B(\mathbf{r}, \tau) &\approx l^z + \bar{l}^z + \mathbf{n}_A \cdot \mathbf{n}_B, \\ \mathbf{d}_B(\mathbf{r}, \tau) \cdot \mathbf{d}_C(\mathbf{r}, \tau) &\approx l^x + \bar{l}^x + \mathbf{n}_B \cdot \mathbf{n}_C, \\ \mathbf{d}_C(\mathbf{r}, \tau) \cdot \mathbf{d}_A(\mathbf{r}, \tau) &\approx l^y + \bar{l}^y + \mathbf{n}_C \cdot \mathbf{n}_A. \end{aligned} \quad (70)$$

Using these approximations, the first term in Eq. (64) can be re-expressed as

$$\begin{aligned} &|\mathbf{d}_A(\mathbf{r}, \tau) \cdot \mathbf{d}_B(\mathbf{r}, \tau)|^2 + |\mathbf{d}_B(\mathbf{r}, \tau) \cdot \mathbf{d}_C(\mathbf{r}, \tau)|^2 \\ &+ |\mathbf{d}_C(\mathbf{r}, \tau) \cdot \mathbf{d}_A(\mathbf{r}, \tau)|^2 \\ &\approx (l^z + \bar{l}^z)^2 + (l^x + \bar{l}^x)^2 + (l^y + \bar{l}^y)^2 \\ &+ |\mathbf{n}_A \cdot \mathbf{n}_B|^2 + |\mathbf{n}_B \cdot \mathbf{n}_C|^2 + |\mathbf{n}_C \cdot \mathbf{n}_A|^2. \end{aligned} \quad (71)$$

Following the same procedure as in Sec. II B results in the Lagrangian

$$\begin{aligned} \mathcal{L}_\Delta^{\text{SU}(2)} &\approx \text{Tr}(\mathbf{U}^\dagger \cdot \partial_\tau \mathbf{U}) + 2[(\mathbf{s} - \bar{\mathbf{s}}) \cdot \mathbf{l}_1 + i(\mathbf{s} + \bar{\mathbf{s}}) \cdot \mathbf{l}_2] \\ &+ 12J_2 \mathbf{l}_1 \cdot \mathbf{l}_1 + 12J_1 \mathbf{l}_2 \cdot \mathbf{l}_2 \\ &+ 3(J_2 - J_1)(|\mathbf{n}_A \cdot \mathbf{n}_B|^2 + |\mathbf{n}_B \cdot \mathbf{n}_C|^2 + |\mathbf{n}_C \cdot \mathbf{n}_A|^2) \\ &+ \text{gradient terms}. \end{aligned} \quad (72)$$

The canting fields \mathbf{l} can once again be eliminated within a saddle-point approximation. Performing the necessary functional derivative and using Eq. (38) to write the result in terms of \mathbf{n} , we find

$$\begin{aligned} \mathbf{l}_1 &\approx -\frac{1}{12J_2} \begin{pmatrix} \bar{\mathbf{n}}_B \cdot \partial_\tau \mathbf{n}_A - \mathbf{n}_B \cdot \partial_\tau \bar{\mathbf{n}}_A \\ \bar{\mathbf{n}}_C \cdot \partial_\tau \mathbf{n}_B - \mathbf{n}_C \cdot \partial_\tau \bar{\mathbf{n}}_B \\ \bar{\mathbf{n}}_A \cdot \partial_\tau \mathbf{n}_C - \mathbf{n}_A \cdot \partial_\tau \bar{\mathbf{n}}_C \end{pmatrix}, \\ \mathbf{l}_2 &\approx -\frac{i}{12J_1} \begin{pmatrix} \bar{\mathbf{n}}_B \cdot \partial_\tau \mathbf{n}_A + \mathbf{n}_B \cdot \partial_\tau \bar{\mathbf{n}}_A \\ \bar{\mathbf{n}}_C \cdot \partial_\tau \mathbf{n}_B + \mathbf{n}_C \cdot \partial_\tau \bar{\mathbf{n}}_B \\ \bar{\mathbf{n}}_A \cdot \partial_\tau \mathbf{n}_C + \mathbf{n}_A \cdot \partial_\tau \bar{\mathbf{n}}_C \end{pmatrix}. \end{aligned} \quad (73)$$

These two canting fields correspond to physically distinct spin- and quadrupole wave excitations. These are no longer degenerate once the SU(3) symmetry is broken, and to parameterize them, we need to introduce two distinct susceptibilities:

$$\chi_\perp^Q = \frac{2}{9J_1}, \quad \chi_\perp^S = \frac{2}{9J_2}, \quad (74)$$

and two distinct director stiffnesses (which for this particular model, happen to be equal),

$$\rho_d^Q = \rho_d^S = J_2 a^2. \quad (75)$$

It also proves convenient to reparametrize the term in $\mathcal{L}_\Delta^{\text{SU}(2)}$, which breaks SU(3) symmetry in terms of a gap to spin-wave excitations, i.e.,

$$\delta \mathcal{L}_\Delta^{\text{SU}(2)} = \frac{3}{8} \chi_\perp^S \Delta^2 (|\mathbf{n}_A \cdot \mathbf{n}_B|^2 + |\mathbf{n}_B \cdot \mathbf{n}_C|^2 + |\mathbf{n}_C \cdot \mathbf{n}_A|^2), \quad (76)$$

where

$$\Delta = \sqrt{36J_2(J_2 - J_1)}. \quad (77)$$

Collecting these facts together, the action describing long-wavelength excitations of three-sublattice AFQ order is

$$\begin{aligned} S_\Delta^{\text{SU}(2)}[\mathbf{n}_A, \bar{\mathbf{n}}_A, \mathbf{n}_B, \bar{\mathbf{n}}_B, \mathbf{n}_C, \bar{\mathbf{n}}_C] &= \frac{1}{4\sqrt{3}} \int_0^\beta d\tau \int d^2r \left\{ \frac{8}{3} \sum_i \bar{\mathbf{n}}_i \cdot \partial_\tau \mathbf{n}_i + \chi_\perp^Q [(\bar{\mathbf{n}}_A \cdot \partial_\tau \mathbf{n}_B + \mathbf{n}_A \cdot \partial_\tau \bar{\mathbf{n}}_B)^2 + (\bar{\mathbf{n}}_B \cdot \partial_\tau \mathbf{n}_C + \mathbf{n}_B \cdot \partial_\tau \bar{\mathbf{n}}_C)^2 \right. \\ &+ (\bar{\mathbf{n}}_C \cdot \partial_\tau \mathbf{n}_A + \mathbf{n}_C \cdot \partial_\tau \bar{\mathbf{n}}_A)^2] - \chi_\perp^S [(\bar{\mathbf{n}}_A \cdot \partial_\tau \mathbf{n}_B - \mathbf{n}_A \cdot \partial_\tau \bar{\mathbf{n}}_B)^2 + (\bar{\mathbf{n}}_B \cdot \partial_\tau \mathbf{n}_C - \mathbf{n}_B \cdot \partial_\tau \bar{\mathbf{n}}_C)^2 \\ &+ (\bar{\mathbf{n}}_C \cdot \partial_\tau \mathbf{n}_A - \mathbf{n}_C \cdot \partial_\tau \bar{\mathbf{n}}_A)^2] + \rho_d^Q \sum_{\lambda=x,y} [(\bar{\mathbf{n}}_A \partial_\lambda \mathbf{n}_B + \mathbf{n}_A \partial_\lambda \bar{\mathbf{n}}_B)^2 + (\bar{\mathbf{n}}_B \partial_\lambda \mathbf{n}_C + \mathbf{n}_B \partial_\lambda \bar{\mathbf{n}}_C)^2 \\ &+ (\bar{\mathbf{n}}_C \partial_\lambda \mathbf{n}_A + \mathbf{n}_C \partial_\lambda \bar{\mathbf{n}}_A)^2] - \rho_d^S \sum_{\lambda=x,y} [(\bar{\mathbf{n}}_A \partial_\lambda \mathbf{n}_B - \mathbf{n}_A \partial_\lambda \bar{\mathbf{n}}_B)^2 + (\bar{\mathbf{n}}_B \partial_\lambda \mathbf{n}_C - \mathbf{n}_B \partial_\lambda \bar{\mathbf{n}}_C)^2 \\ &+ (\bar{\mathbf{n}}_C \partial_\lambda \mathbf{n}_A - \mathbf{n}_C \partial_\lambda \bar{\mathbf{n}}_A)^2] + \chi_\perp^S \Delta^2 (|\mathbf{n}_A \cdot \mathbf{n}_B|^2 + |\mathbf{n}_B \cdot \mathbf{n}_C|^2 + |\mathbf{n}_C \cdot \mathbf{n}_A|^2) \left. \right\}, \end{aligned} \quad (78)$$

where the relevant parameters for the microscopic model $\mathcal{H}_\Delta^{\text{BBQ}}$ [see Eq. (1)] are given in Table I, and the partition function is defined as in Eq. (48).

Equation (25) can be used to re-express this action in terms of the unitary matrix field $\mathbf{U}(\mathbf{r}, \tau)$ as

$$\begin{aligned} \mathcal{S}_\Delta^{\text{SU}(2)}[\mathbf{U}] = & \frac{1}{8\sqrt{3}a^2} \int_0^\beta d\tau \int d^2r \left\{ \frac{16}{3} \text{Tr}(\mathbf{U}^\dagger \cdot \partial_\tau \mathbf{U}) + \chi_\perp^{\text{Q}} \text{Tr}(\mathbf{U}^\dagger \cdot \partial_\tau \mathbf{U} + \mathbf{U}^{\text{T}} \cdot \partial_\tau \bar{\mathbf{U}})^\dagger (\mathbf{U}^\dagger \cdot \partial_\tau \mathbf{U} + \mathbf{U}^{\text{T}} \cdot \partial_\tau \bar{\mathbf{U}}) \right. \\ & + \chi_\perp^{\text{S}} \left[\text{Tr}(\mathbf{U}^\dagger \cdot \partial_\tau \mathbf{U} - \mathbf{U}^{\text{T}} \cdot \partial_\tau \bar{\mathbf{U}})^\dagger (\mathbf{U}^\dagger \cdot \partial_\tau \mathbf{U} - \mathbf{U}^{\text{T}} \cdot \partial_\tau \bar{\mathbf{U}}) - 4 \sum_m |(\mathbf{U}^\dagger \cdot \partial_\tau \mathbf{U})_{mm}|^2 \right] \\ & + \rho_{\text{d}}^{\text{Q}} \text{Tr}(\mathbf{U}^\dagger \cdot \partial_\lambda \mathbf{U} + \mathbf{U}^{\text{T}} \cdot \partial_\lambda \bar{\mathbf{U}})^\dagger (\mathbf{U}^\dagger \cdot \partial_\lambda \mathbf{U} + \mathbf{U}^{\text{T}} \cdot \partial_\lambda \bar{\mathbf{U}}) + \rho_{\text{d}}^{\text{S}} \left[\text{Tr}(\mathbf{U}^\dagger \cdot \partial_\lambda \mathbf{U} - \mathbf{U}^{\text{T}} \cdot \partial_\lambda \bar{\mathbf{U}})^\dagger (\mathbf{U}^\dagger \cdot \partial_\lambda \mathbf{U} - \mathbf{U}^{\text{T}} \cdot \partial_\lambda \bar{\mathbf{U}}) \right. \\ & \left. \left. - 4 \sum_m |(\mathbf{U}^\dagger \cdot \partial_\tau \mathbf{U})_{mm}|^2 \right] + \chi_\perp^{\text{S}} \Delta^2 \left[3 - \sum_i |(\mathbf{U}^{\text{T}} \cdot \mathbf{U})_{mm}|^2 \right] \right\}. \end{aligned} \quad (79)$$

This reduces to Eq. (49) when $\chi_\perp^{\text{Q}} = \chi_\perp^{\text{S}}$ and $\Delta = 0$ (i.e., $J_1 = J_2$), as required.

2. Linearizing the order parameter fields

The physical content of the action $\mathcal{S}_\Delta^{\text{SU}(2)}[\mathbf{n}]$ [see Eq. (78)] becomes clear on linearization of the fields. Once again, we use Eq. (51) to expand small fluctuations about the ground state in terms of ϕ . This leads to the action

$$\begin{aligned} \mathcal{S}_\Delta^{\text{SU}(2)}[\phi] \approx & \frac{1}{\sqrt{3}a^2} \int_0^\beta d\tau \int d^2r \sum_{p=1\dots 3} \left[\chi_\perp^{\text{Q}} (\partial_\tau \phi_p)^2 \right. \\ & \left. + \rho_{\text{d}}^{\text{Q}} \sum_{\lambda=x,y} (\partial_\lambda \phi_p)^2 \right] + \sum_{p=4\dots 6} \left[\chi_\perp^{\text{S}} (\partial_\tau \phi_p)^2 \right. \\ & \left. + \rho_{\text{d}}^{\text{S}} \sum_{\lambda=x,y} (\partial_\lambda \phi_p)^2 + \chi_\perp^{\text{S}} \Delta^2 \phi_p^2 \right]. \end{aligned} \quad (80)$$

We immediately see that there are three gapless, quadrupole-wave modes, ϕ_1 , ϕ_2 , and ϕ_3 , with dispersion

$$\omega_{\mathbf{q}}^{\text{Q}} \approx v_{\text{Q}} |\mathbf{q}|, \quad v_{\text{Q}} = \sqrt{\frac{\rho_{\text{d}}^{\text{Q}}}{\chi_\perp^{\text{Q}}}} = 3\sqrt{\frac{J_1 J_2}{2}} a, \quad (81)$$

and three gapped, spin-wave modes ϕ_4 , ϕ_5 , and ϕ_6 , with dispersion

$$\omega_{\mathbf{q}}^{\text{S}} \approx \sqrt{\Delta^2 + v_{\text{S}}^2 \mathbf{q}^2}, \quad v_{\text{S}} = \sqrt{\frac{\rho_{\text{d}}^{\text{S}}}{\chi_\perp^{\text{S}}}} = 3\frac{J_2 a}{\sqrt{2}}. \quad (82)$$

TABLE I. Dictionary for translating between the parameters of the continuum field theory for three-sublattice AFQ order, $\mathcal{S}_\Delta^{\text{SU}(2)}[\mathbf{U}]$ [see Eq. (79)] and the parameters of the relevant microscopic model $\mathcal{H}_\Delta^{\text{BBQ}}$ [see Eq. (1)], in the vicinity of the SU(3) point $J_1 = J_2$.

$\mathcal{S}_\Delta^{\text{SU}(2)}[\mathbf{U}]$	$\mathcal{H}_\Delta^{\text{BBQ}}$
χ_\perp^{Q}	$2/(9J_1)$
χ_\perp^{S}	$2/(9J_2)$
$\rho_{\text{d}}^{\text{Q}}$	$J_2 a^2$
$\rho_{\text{d}}^{\text{S}}$	$J_2 a^2$
Δ	$\sqrt{36J_2(J_2 - J_1)}$

These are shown in Fig. 11. The Goldstone modes correspond to real rotations of the order parameter fields, while the gapped modes (gap Δ) correspond to rotations into complex space.

The microscopic ‘‘flavor wave’’ theory developed by Tsunetsugu and Arikawa^{40,41} predicts a dispersion

$$\omega_{\mathbf{k}}^\pm = 3J_2 \sqrt{(1 \pm |\gamma_{\mathbf{k}}|) \left[1 \pm \left(1 - \frac{2J_1}{J_2} \right) |\gamma_{\mathbf{k}}| \right]}, \quad (83)$$

where $\gamma_{\mathbf{k}}$ is given by Eq. (61). This is shown in Fig. 9. In the long wavelength limit, and for small $J_2 - J_1$, the dispersion reduces to Eqs. (81) and (82).

We re-emphasize that the validity of the continuum theory breaks down approaching the FM phase for $\theta \rightarrow \pi/2$ ($J_1 \rightarrow 0$, $J_2 > 0$). Crossing the AFQ phase, there is a progressive reduction in the area of reciprocal space over which the quadrupole-wave dispersion, $\omega_{\mathbf{k}}^-$, is linear. This is also a feature of the lattice theory—exactly at the phase boundary with the ferromagnet ($J_1 = 0$, $J_2 > 0$) the dispersion, $\omega_{\mathbf{k}}^\pm$ [see Eq. (83)], becomes quadratic even for $|\mathbf{k}| \rightarrow 0$. This signals that it is no longer appropriate to describe the system in terms of the quantum nonlinear σ model, $\mathcal{S}_\Delta^{\text{SU}(2)}[\mathbf{U}]$ [see Eq. (79)].

E. The low-temperature, low-energy limit

For temperature and energy scales lower than the spin-wave gap Δ the high-energy, spin-wave modes can be neglected. This considerably simplifies the action, $\mathcal{S}_\Delta^{\text{SU}(2)}[\mathbf{n}]$ [see Eq. (78)], and is a useful approximation when considering low temperature thermodynamic properties.

Neglecting of the spin-wave modes is equivalent to making the assumption that the fields \mathbf{n}_i are real. The simplified action is then given by

$$\begin{aligned} \mathcal{S}_\Delta^{\text{SO}(3)}[\mathbf{n}_\mathbf{A}, \mathbf{n}_\mathbf{B}, \mathbf{n}_\mathbf{C}] \\ \approx & \frac{1}{2\sqrt{3}a^2} \int_0^\beta d\tau \int d^2r \left\{ \chi_\perp^{\text{Q}} [(\partial_\tau \mathbf{n}_\mathbf{A})^2 + (\partial_\tau \mathbf{n}_\mathbf{B})^2 \right. \\ & \left. + (\partial_\tau \mathbf{n}_\mathbf{C})^2] + \rho_{\text{d}}^{\text{Q}} \sum_{\lambda=x,y} [(\partial_\lambda \mathbf{n}_\mathbf{A})^2 + (\partial_\lambda \mathbf{n}_\mathbf{B})^2 + (\partial_\lambda \mathbf{n}_\mathbf{C})^2] \right\}, \end{aligned} \quad (84)$$

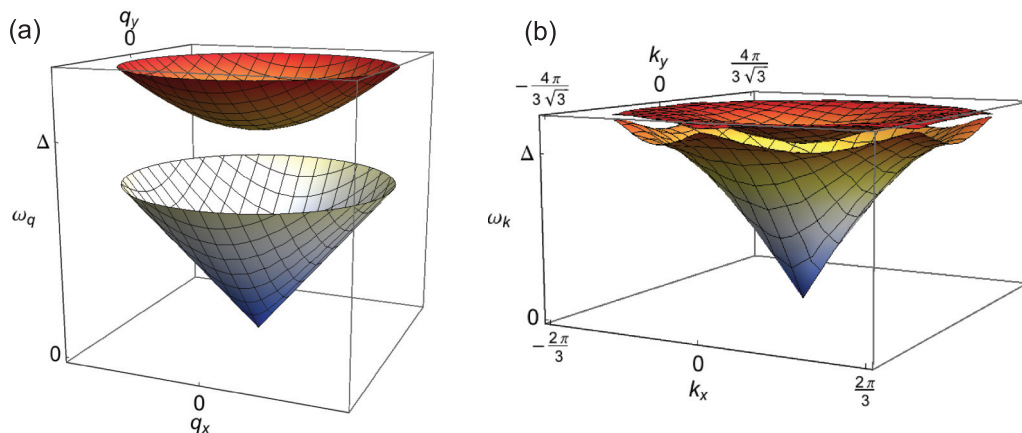


FIG. 11. (Color online) Dispersion of magnetic excitations in a three-sublattice antiferroquadrupolar (AFQ) spin-nematic state on a triangular lattice. (a) Prediction of the continuum field theory $\mathcal{S}_\Delta^{\text{SU}(2)}[\phi]$ [see Eq. (80)], with dispersion given by ω_q^{Q} [see Eq. (81)] and ω_q^{S} [see Eq. (82)]. (b) Prediction of the microscopic model $\mathcal{H}_\Delta^{\text{BBQ}}$ [see Eq. (1)] in the magnetic Brillouin zone (mbz) [see Fig. 10], for parameters $J_1 = 1$ and $J_2 = 1.22$. The dispersion is given by ω_q^{\pm} [see Eq. (83)]. In both cases, a threefold degenerate branch of gapless, quadrupole-wave excitations, are centered on the ordering vector $\mathbf{k} = \mathbf{k}_K$ [i.e., $\mathbf{q} = 0$]. These are the Goldstone modes of the AFQ order. They are accompanied by a threefold degenerate branch of gapped, spin-wave excitations. Approaching the center of the mbz, $\mathbf{q} \rightarrow 0$, the continuum theory and the lattice theory match exactly.

with canting field

$$\mathbf{l} \approx i\mathbf{l}_2 \approx \frac{3}{4}\chi_\perp^{\text{Q}} \begin{pmatrix} \mathbf{n}_B \cdot \partial_\tau \mathbf{n}_A \\ \mathbf{n}_C \cdot \partial_\tau \mathbf{n}_B \\ \mathbf{n}_A \cdot \partial_\tau \mathbf{n}_C \end{pmatrix} \quad (85)$$

and the partition function is

$$\mathcal{Z}_\Delta^{\text{SO}(3)} \propto \int \prod_{i \neq j} \mathcal{D}\mathbf{n}_i \delta(\mathbf{n}_i^2 - 1) \delta(\mathbf{n}_i \cdot \mathbf{n}_j) e^{-S_\Delta^{\text{SU}(2)}[\mathbf{n}_A, \mathbf{n}_B, \mathbf{n}_C]}. \quad (86)$$

This is an $\text{SO}(3)$ symmetric nonlinear σ model,⁷⁶ a fact which is clearer if the action is written in matrix form:

$$S_\Delta^{\text{SO}(3)}[\mathbf{R}] \approx \frac{1}{2\sqrt{3}a^2} \int_0^\beta d\tau \int d^2r \left[\chi_\perp^{\text{Q}} \text{Tr}(\partial_\tau \mathbf{R}^T \cdot \partial_\tau \mathbf{R}) + \rho_d^{\text{Q}} \sum_{\lambda=x,y} \text{Tr}(\partial_\lambda \mathbf{R}^T \cdot \partial_\lambda \mathbf{R}) \right], \quad (87)$$

where \mathbf{R} is a real-valued rotation matrix given by

$$\mathbf{R}(\mathbf{r}, \tau) = \begin{pmatrix} n_A^x(\mathbf{r}, \tau) & n_B^x(\mathbf{r}, \tau) & n_C^x(\mathbf{r}, \tau) \\ n_A^y(\mathbf{r}, \tau) & n_B^y(\mathbf{r}, \tau) & n_C^y(\mathbf{r}, \tau) \\ n_A^z(\mathbf{r}, \tau) & n_B^z(\mathbf{r}, \tau) & n_C^z(\mathbf{r}, \tau) \end{pmatrix}. \quad (88)$$

The simplified action, Eq. (84), describes the three quadrupole-wave modes shown in Fig. 11 but ignores the three spin-wave modes, which dominate experimental responses at higher energy.

F. Comparison with other forms of magnetic order

It is interesting to compare the continuum theory of long-wavelength excitations in a three-sublattice AFQ state, $\mathcal{S}_\Delta^{\text{SU}(2)}[\mathbf{U}]$ [see Eq. (79)], with σ -model approaches to other forms of magnetic order. Perhaps the most widely known example is the σ -model treatment of the collinear antiferromagnet (AFM).^{72–75} The collinear nature of this state means

that it does not break the full $\text{SU}(2)$ spin-rotation symmetry, but instead $\text{SU}(2)/\text{U}(1)$. As a consequence, the resulting σ model describes only two, degenerate, linearly dispersing Goldstone modes, both with the character of spin-wave excitations. The only gapped excitation possible at long wavelength is a longitudinal fluctuation of the order parameter, explicitly absent from the σ model. Collinearity also imposes constraints on the interactions that can arise between different spin excitations, restricting these to vertices involving an even number of excitations.

The key features of the continuum theory of three-sublattice AFQ order, $\mathcal{S}_\Delta^{\text{SU}(2)}[\mathbf{U}]$ [see Eq. (79)], are three degenerate, linearly dispersing “quadrupole-wave” modes associated with the breaking of spin-rotation symmetry, and three degenerate, gapped “spin-wave” modes, associated with dipolar excitations of the underlying quadrupolar order. The two actions therefore differ in both the number and the character of the modes they describe. It is also worth noting that the structure of the interactions between these excitations (not described in this article) is profoundly different and includes vertices with an odd number of excitations. This topic will be explored further elsewhere.⁶³

The action $\mathcal{S}_\Delta^{\text{SU}(2)}[\mathbf{U}]$ [see Eq. (79)] finds more parallels with noncollinear magnetic ordering. A good example of this is the 120° state on the triangular lattice.^{70,71} This fully breaks the $\text{SU}(2)$ symmetry, and therefore has three, linearly dispersing Goldstone modes, all with the character of spin waves. Interactions between odd numbers of spin excitations are also now permitted by symmetry. However, as with the collinear antiferromagnet, the 120° state has no low-energy gapped modes at long wavelength. Also, the coplanar nature of this state means that the spin stiffness’ associated with the three Goldstone modes are not all equal, and only two of the three Goldstone modes are degenerate.

Finally, it is interesting to compare $\mathcal{S}_\Delta^{\text{SU}(2)}[\mathbf{U}]$ [see Eq. (79)] with field theories describing FQ order.^{59–62} As with the

collinear AFM, FQ states have only two Goldstone modes. These are degenerate, linearly dispersing, and have the character of quadrupole waves at long wavelength. Only interactions between even numbers of spin excitations are permitted by symmetry. Both of these points clearly distinguish the present theory of AFQ order from the earlier work on FQ order.

In fact, the theory derived in Ref. 59 has the same action as the collinear AFM, albeit with a different physical interpretation. However, in reducing the action to this form, imaginary fluctuations of the director \mathbf{d} have been explicitly integrated out, eliminating much of the information concerning excitations with “spin-wave” character. An important feature of the SU(3)-derived approach developed in this article is its ability to describe gapped excitations with dipolar character,

such as the “spin-wave” modes of AFQ order, which *cannot* be accessed in the SO(3) approach of Ref. 59. Such modes are particularly interesting since they will be the easiest to observe in, e.g., inelastic neutron scattering.

G. Machinery for calculating correlation functions

In order to make predictions for inelastic neutron scattering and for the dynamical quadrupole susceptibility, it is necessary to translate the continuum field theory, $\mathcal{S}_{\Delta}^{\text{SU}(2)}[\mathbf{U}]$ [see Eq. (79)]—which is written in terms of rotations of directors—back into the language of spins and quadrupoles. Following Eqs. (24) and (50), the directors on the three sublattices can be approximated as

$$\mathbf{d}_A \approx \begin{pmatrix} 1 \\ -\phi_1 + i\phi_4 + \bar{l}^z \\ \phi_2 + i\phi_5 + l^y \end{pmatrix}, \quad \mathbf{d}_B \approx \begin{pmatrix} \phi_1 + i\phi_4 + l^z \\ 1 \\ -\phi_3 + i\phi_6 + \bar{l}^x \end{pmatrix}, \quad \mathbf{d}_C \approx \begin{pmatrix} -\phi_2 + i\phi_5 + \bar{l}^y \\ \phi_3 + i\phi_6 + l^x \\ 1 \end{pmatrix}, \quad (89)$$

with the canting fields

$$\mathbf{l}_1 \approx -\frac{3}{4}\chi_{\perp}^{\text{S}} \begin{pmatrix} \partial_t \phi_4 \\ \partial_t \phi_6 \\ \partial_t \phi_5 \end{pmatrix}, \quad \mathbf{l}_2 \approx \frac{3}{4}\chi_{\perp}^{\text{Q}} \begin{pmatrix} \partial_t \phi_1 \\ \partial_t \phi_3 \\ \partial_t \phi_2 \end{pmatrix}, \quad (90)$$

where the real time $t = -i\tau$ has been used. It follows that the \mathbf{d} vectors are

$$\mathbf{d}_A \approx \begin{pmatrix} 1 \\ -\phi_1 + i\phi_4 - \frac{3}{4}\chi_{\perp}^{\text{S}}\partial_t\phi_4 - i\frac{3}{4}\chi_{\perp}^{\text{Q}}\partial_t\phi_1 \\ \phi_2 + i\phi_5 - \frac{3}{4}\chi_{\perp}^{\text{S}}\partial_t\phi_5 + i\frac{3}{4}\chi_{\perp}^{\text{Q}}\partial_t\phi_2 \end{pmatrix}, \quad \mathbf{d}_B \approx \begin{pmatrix} \phi_1 + i\phi_4 - \frac{3}{4}\chi_{\perp}^{\text{S}}\partial_t\phi_4 + i\frac{3}{4}\chi_{\perp}^{\text{Q}}\partial_t\phi_1 \\ 1 \\ -\phi_3 + i\phi_6 - \frac{3}{4}\chi_{\perp}^{\text{S}}\partial_t\phi_6 - i\frac{3}{4}\chi_{\perp}^{\text{Q}}\partial_t\phi_3 \end{pmatrix}, \quad (91)$$

$$\mathbf{d}_C \approx \begin{pmatrix} -\phi_2 + i\phi_5 - \frac{3}{4}\chi_{\perp}^{\text{S}}\partial_t\phi_5 - i\frac{3}{4}\chi_{\perp}^{\text{Q}}\partial_t\phi_2 \\ \phi_3 + i\phi_6 - \frac{3}{4}\chi_{\perp}^{\text{S}}\partial_t\phi_6 + i\frac{3}{4}\chi_{\perp}^{\text{Q}}\partial_t\phi_3 \\ 1 \end{pmatrix}.$$

Substituting these expressions into Eq. (14) leads to the fluctuating dipole moments:

$$\mathbf{S}_A \approx \begin{pmatrix} 0 \\ -2\phi_5 - \frac{3}{2}\chi_{\perp}^{\text{Q}}\partial_t\phi_2 \\ 2\phi_4 - \frac{3}{2}\chi_{\perp}^{\text{Q}}\partial_t\phi_1 \end{pmatrix}, \quad \mathbf{S}_B \approx \begin{pmatrix} 2\phi_6 - \frac{3}{2}\chi_{\perp}^{\text{Q}}\partial_t\phi_3 \\ 0 \\ -2\phi_4 - \frac{3}{2}\chi_{\perp}^{\text{Q}}\partial_t\phi_1 \end{pmatrix}, \quad \mathbf{S}_C \approx \begin{pmatrix} -2\phi_6 - \frac{3}{2}\chi_{\perp}^{\text{Q}}\partial_t\phi_3 \\ 2\phi_5 - \frac{3}{2}\chi_{\perp}^{\text{Q}}\partial_t\phi_2 \\ 0 \end{pmatrix}, \quad (92)$$

where terms linear in the ϕ fields have been retained. Equation (92) provides the starting point for the theory of inelastic neutron scattering developed in Sec. III of this paper.

The quadrupole moments are given by

$$\mathbf{Q}_A \approx \begin{pmatrix} -1 \\ \frac{1}{\sqrt{3}} \\ -2\phi_1 - \frac{3}{2}\chi_{\perp}^{\text{S}}\partial_t\phi_4 \\ 0 \\ -2\phi_2 + \frac{3}{2}\chi_{\perp}^{\text{S}}\partial_t\phi_5 \end{pmatrix}, \quad \mathbf{Q}_B \approx \begin{pmatrix} 1 \\ \frac{1}{\sqrt{3}} \\ 2\phi_1 - \frac{3}{2}\chi_{\perp}^{\text{S}}\partial_t\phi_4 \\ -2\phi_3 - \frac{3}{2}\chi_{\perp}^{\text{S}}\partial_t\phi_6 \\ 0 \end{pmatrix}, \quad \mathbf{Q}_C \approx \begin{pmatrix} 0 \\ -\frac{2}{\sqrt{3}} \\ 0 \\ 2\phi_3 - \frac{3}{2}\chi_{\perp}^{\text{S}}\partial_t\phi_6 \\ 2\phi_2 + \frac{3}{2}\chi_{\perp}^{\text{S}}\partial_t\phi_5 \end{pmatrix}. \quad (93)$$

References 64 and 65 contain animations showing the nature of the quadrupole-wave⁶⁴ and spin-wave⁶⁵ excitations.

III. PREDICTIONS FOR INELASTIC NEUTRON SCATTERING

A. General considerations: waves in the unseen

Since each “spin” in a quantum magnet possesses a magnetic dipole, conventional *dipolar* magnetic order gives

rise to a static internal magnetic field. Neutrons, which also possess a dipole moment, diffract from this static field to give magnetic Bragg peaks. As in conventional crystallography, the form of magnetic order present is encoded in the wave number and intensity of these magnetic Bragg peaks. However, since spin-nematic order corresponds to a *quadrupolar* order

of spins, it does *not* break time-reversal symmetry and *cannot* give rise to static magnetic fields.^{4,9} For this reason, it does not manifest itself through magnetic Bragg peaks in elastic neutron scattering.

An elegant solution to this problem, *in the presence of an anisotropy* that breaks SU(2) symmetry, was proposed by Barzykin and Gorkov,⁸ who suggested using an external magnetic field to break time-reversal symmetry. In the presence of magnetic anisotropy, applying a uniform magnetic field to an AFQ state induces a small, staggered, dipole moment, which can, in principle, be observed in elastic neutron scattering. Resonant magnetic x-ray scattering, which *is* sensitive to quadrupole moments of spins, has also been used to identify AFQ order in the rare-earth magnet UPd₃⁷⁷⁻⁷⁹ However, a very direct and appealing route to identifying spin-nematic order, even in the absence of magnetic anisotropy, would be to map out its magnetic excitations using inelastic neutron scattering.

Since spin-nematic order breaks spin-rotation symmetry, it *must* possess Goldstone modes. The long-wavelength excitations are generated by real SU(2) rotations of the underlying quadrupolar order parameter, and so can best be thought of as “quadrupole waves.” Quadrupole waves possess a small fluctuating dipole moment, and will reveal themselves as linearly dispersing excitations—visible waves in the unseen spin-nematic order. As we will see in what follows, the size of this dipole moment is directly proportional to the speed at which the quadrupoles rotate, and so the intensity of scattering from a quadrupole wave vanishes linearly with its energy.

However, precisely because the building blocks of spin-nematic order are quadrupole moments of spins, these Goldstone modes do *not* exhaust the possible excitations of a spin-nematic state. Neutrons can also drive transitions between different triplet states, which mix a strong spin-dipole into the underlying quadrupole moment. In AFQ spin-nematic states, this leads to a second, distinct, type of long-wavelength excitation, with a gapped spectrum and a pronounced intensity in inelastic neutron scattering. Identifying this gapped excitation in experiment, together with the appropriate set of gapless Goldstone modes, would provide strong evidence for the existence of spin-nematic order.

In Sec. II of this paper, we have developed the tools needed to make distinctive, quantitative predictions for *both* types of excitation of a spin-nematic—a continuum field-theory of the excitations of AFQ order based on the symmetries of the underlying order parameter. This SU(3) “ σ -model” approach offers a *quantitative* description of excitations—in terms of the minimum set of physically meaningful parameters—*without* the need to specify a microscopic model.

In what follows, we use this continuum theory to make predictions for inelastic neutron scattering carried out on a three-sublattice AFQ state. These predictions are *exact* at long wavelength, and fully constrain the symmetries broken by the AFQ state. We make explicit comparison with the predictions of a microscopic, spin-1 lattice model that realizes the same ordered state. In order to keep the discussion reasonably self-contained, key results from Sec. II are quoted in the text.

B. Sum rules and correlation functions

Inelastic neutron scattering measures the imaginary part of the dynamical spin susceptibility

$$\Im m \{ \chi_S^{\alpha\beta}(\mathbf{k}, \omega) \} = (g\mu_B)^2 \Im m \left\{ i \int_0^\infty dt e^{i\omega t} \langle \delta S^\alpha(\mathbf{k}, t) \delta S^\beta(-\mathbf{k}, 0) \rangle \right\}, \quad (94)$$

where $\alpha, \beta = x, y, z$ label spin components. In the case of the three-sublattice AFQ state described in Sec. II, this tensor is diagonal, and fluctuations are isotropic in spin space, i.e., ,

$$\Im m \{ \chi_S^{xx}(\mathbf{k}, \omega) \} = \Im m \{ \chi_S^{yy}(\mathbf{k}, \omega) \} = \Im m \{ \chi_S^{zz}(\mathbf{k}, \omega) \}.$$

An important check on any calculation of the dynamical susceptibility is that it obeys the relevant sum rules. For any theory with SU(2) spin symmetry, as is the case for the three-sublattice AFQ state, it is required that

$$\lim_{\mathbf{k} \rightarrow 0} \int d\omega e^{i\omega t} \omega \chi_S^{\alpha\beta}(\mathbf{k}, \omega) = 0. \quad (95)$$

This says that at $\mathbf{k} = 0$, the dynamical susceptibility must vanish for all $\omega \neq 0$. The sum rule is related to a Ward-Takahashi identity, and thus holds at *each* order in perturbation theory. For single particle excitations, it is sufficient to consider the noninteracting theory described by $\mathcal{H}_\Delta^{\text{SU}(2)}[\phi]$ [see Eq. (80)]. However, in order to understand the 2-particle continuum it is necessary to take three and four field interactions into account and form a Dyson equation for the self energy. Since this is an involved process, we postpone discussion until a future publication.⁶³ We note that the linear flavor wave analysis of Tsunetsugu and Arikawa⁴⁰ obeys the sum rule, Eq. (97), at leading order, but has finite weight at $\mathbf{k} = 0$ and $\omega \neq 0$ arising from the 2-particle continuum.

In Sec. IV, we also consider the dynamical quadrupole susceptibility. This is given by

$$\Im m \{ \chi_Q^{\alpha\beta\gamma\delta}(\mathbf{k}, \omega) \} = (g\mu_B)^4 \Im m \left\{ i \int_0^\infty dt e^{i\omega t} \langle \delta Q^{\alpha\beta}(\mathbf{k}, t) \delta Q^{\gamma\delta}(-\mathbf{k}, 0) \rangle \right\}. \quad (96)$$

In the general case of SU(2) spin symmetry, there is no analogous sum rule to Eq. (97), and one expects to find finite weight at $\mathbf{k} = 0$ and $\omega \neq 0$. However, exactly at the SU(3) point, the expanded symmetry leads to the quadrupolar sum rule

$$\lim_{\mathbf{k} \rightarrow 0} \int d\omega e^{i\omega t} \omega \chi_Q^{\alpha\beta}(\mathbf{k}, \omega) = 0 \quad [\text{SU}(3) \text{ point}]. \quad (97)$$

C. Neutron scattering in a three-sublattice AFQ

1. Spin excitations in a three-sublattice AFQ state

Predictions for inelastic neutron scattering from a three-sublattice AFQ state have previously been published by Tsunetsugu and Arikawa,^{40,41} based on flavorwave calculations for the spin-1 bilinear-biquadratic (BBQ) model on the triangular lattice $\mathcal{H}_\Delta^{\text{BBQ}}$ [see Eq. (1)]. In what follows we show how the universal, long-wavelength features of these results are completely described by the field theory developed in Sec. II

of this paper. The tools needed to calculate $\Im m\{\chi_S^{\alpha\beta}(\mathbf{k}, \omega)\}$ —namely, a theory of long-wavelength spin excitations in a spin-nematic state—were developed in Sect. II of this paper. Here, we briefly reprice the most relevant results.

Small fluctuations about the three-sublattice AFQ ordered state can be described by the linearized action, $\mathcal{S}_\Delta^{\text{SU}(2)}[\boldsymbol{\phi}]$ [see Eq. (80)], viz.,

$$\mathcal{S}_\Delta^{\text{SU}(2)}[\boldsymbol{\phi}] \approx \frac{1}{\sqrt{3}a^2} \int_0^\beta d\tau \int d^2r \sum_{p=1\dots 3} \left[\chi_\perp^{\text{Q}} (\partial_\tau \phi_p)^2 + \rho_{\text{d}}^{\text{Q}} \sum_{\lambda=x,y} (\partial_\lambda \phi_p)^2 \right] + \sum_{p=4\dots 6} \left[\chi_\perp^{\text{S}} (\partial_\tau \phi_p)^2 + \rho_{\text{d}}^{\text{S}} \sum_{\lambda=x,y} (\partial_\lambda \phi_p)^2 + \chi_\perp^{\text{S}} \Delta^2 \phi_p^2 \right].$$

The long-wavelength properties of the three-sublattice AFQ state are completely characterized by the four parameters χ_\perp^{Q} , χ_\perp^{S} , $\rho_{\text{d}}^{\text{Q}} = \rho_{\text{d}}^{\text{S}}$ and Δ . Table I provides a “dictionary” for converting between the parameters of the continuum theory, and the parameters of the minimal microscopic model $\mathcal{H}_\Delta^{\text{BBQ}}$ [see Eq. (1)].

The dispersion of the spin excitations of this spin-nematic state then follow from the usual Euler-Lagrange equations. The three fields ϕ_1 , ϕ_2 , and ϕ_3 describe Goldstone modes with linear dispersion $\omega_{\mathbf{q}}^{\text{Q}}$ [see Eq. (81)], viz.,

$$\omega_{\mathbf{q}}^{\text{Q}} \approx v_{\text{Q}} |\mathbf{q}|, \quad v_{\text{Q}} = \sqrt{\frac{\rho_{\text{d}}^{\text{Q}}}{\chi_\perp^{\text{Q}}}},$$

while the three fields ϕ_4 , ϕ_5 , and ϕ_6 , describe gapped excitations with dispersion $\omega_{\mathbf{q}}^{\text{S}}$ [see Eq. (82)], viz.,

$$\omega_{\mathbf{q}}^{\text{S}} \approx \sqrt{\Delta^2 + v_{\text{S}}^2 \mathbf{q}^2}, \quad v_{\text{S}} = \sqrt{\frac{\rho_{\text{d}}^{\text{S}}}{\chi_\perp^{\text{S}}}}.$$

The remaining challenge is to correctly reference the continuum theory back to the lattice, and to calculate the intensities associated with each branch of excitation. To do this it is necessary to transcribe the spin degrees of freedom (S^x, S^y, S^z) in terms of the fields $\boldsymbol{\phi}$, and then decompose spin-spin correlations $\langle S^\alpha S^\beta \rangle$ as contractions of the $\boldsymbol{\phi}$ fields. These can contain contributions from more than one kind of excitation. A worked example of this type of calculation is given in Appendix A of Ref. 80.

It follows from Eq. (92) [see Sec. II G] that, to leading order in ϕ ,

$$\delta \mathbf{S}(\mathbf{r}, t) \approx -\frac{\chi_\perp^{\text{Q}}}{2} \begin{pmatrix} (2 - e^{i\mathbf{k}_K \cdot \mathbf{r}} - e^{-i\mathbf{k}_K \cdot \mathbf{r}}) \partial_t \phi_3 \\ [2 + (1 + e^{-i\frac{2\pi}{3}}) e^{i\mathbf{k}_K \cdot \mathbf{r}} + (1 + e^{i\frac{2\pi}{3}}) e^{-i\mathbf{k}_K \cdot \mathbf{r}}] \partial_t \phi_2 \\ [2 + (1 + e^{i\frac{2\pi}{3}}) e^{i\mathbf{k}_K \cdot \mathbf{r}} + (1 + e^{-i\frac{2\pi}{3}}) e^{-i\mathbf{k}_K \cdot \mathbf{r}}] \partial_t \phi_1 \end{pmatrix} + \frac{2}{3} \begin{pmatrix} (e^{i\frac{2\pi}{3}} - e^{-i\frac{2\pi}{3}}) (e^{i\mathbf{k}_K \cdot \mathbf{r}} - e^{-i\mathbf{k}_K \cdot \mathbf{r}}) \phi_6 \\ [(-1 + e^{-i\frac{2\pi}{3}}) e^{i\mathbf{k}_K \cdot \mathbf{r}} + (-1 + e^{i\frac{2\pi}{3}}) e^{-i\mathbf{k}_K \cdot \mathbf{r}}] \phi_5 \\ [(1 - e^{i\frac{2\pi}{3}}) e^{i\mathbf{k}_K \cdot \mathbf{r}} + (1 - e^{-i\frac{2\pi}{3}}) e^{-i\mathbf{k}_K \cdot \mathbf{r}}] \phi_4 \end{pmatrix}. \quad (98)$$

From Eq. (98), we can immediately identify the three fields ϕ_1 , ϕ_2 , and ϕ_3 with quadrupole waves whose contribution to scattering vanishes as $\chi_\perp^{\text{Q}} \partial_t \phi \sim \chi_\perp^{\text{Q}} \omega_{\mathbf{q}}^{\text{Q}}$. Meanwhile, the three fields ϕ_4 , ϕ_5 , and ϕ_6 are spin waves with a robust dipole moment.

2. Single-particle scattering near to $\mathbf{k} = \mathbf{k}_K$

Let us consider first scattering involving a single excitation near to the ordering vector, $\mathbf{k} = \mathbf{k}_K$. Here the field theory predicts a gapless Goldstone mode with dispersion $\omega_{\mathbf{q}}^{\text{Q}}$ [see Eq. (81)], for small $\mathbf{q} = \mathbf{k} - \mathbf{k}_K$. This is accompanied by a gapped spin-wave excitation with dispersion $\omega_{\mathbf{q}}^{\text{S}}$ [see Eq. (82)]. The associated single-particle contribution to the dynamical susceptibility is

$$\Im m\{\chi_S^{\text{xx}}(\mathbf{k}_K + \mathbf{q}, \omega)\} \approx \frac{\pi}{8} (g\mu_{\text{B}})^2 \chi_\perp^{\text{Q}} \omega_{\mathbf{q}}^{\text{Q}} \delta(\omega - \omega_{\mathbf{q}}^{\text{Q}}) + \frac{2\pi}{3} (g\mu_{\text{B}})^2 \frac{1}{\chi_\perp^{\text{S}} \omega_{\mathbf{q}}^{\text{S}}} \delta(\omega - \omega_{\mathbf{q}}^{\text{S}}), \quad (99)$$

where $\mathbf{q} \approx 0$. Scattering close to the K' point is exactly equivalent. From Eq. (99), we see that the intensity of scattering from the quadrupole wave vanishes as $\chi_\perp^{\text{Q}} \omega_{\mathbf{q}}^{\text{Q}} \sim \chi_\perp^{\text{Q}} v_{\text{Q}} |\mathbf{q}|$ for $\mathbf{q} \rightarrow 0$. Meanwhile, the scattering from the spin-wave excitation is enhanced as $1/(\chi_\perp^{\text{S}} \omega_{\mathbf{q}}^{\text{S}}) \sim 1/(\Delta \chi_\perp^{\text{S}})$ in the same limit. The spin-wave excitation will therefore dominate the response seen in experiment. These features are illustrated in Fig. 12.

Exactly the same quadrupole and spin-wave excitations are found in flavor wave calculations^{40,41} for the three-sublattice AFQ phase of the spin-1 BBQ model on the triangular lattice \mathcal{H}_{BBQ} [see Eq. (1)]. These predict a 1-particle contribution to the dynamical susceptibility which behaves as

$$\Im m\{\chi_S^{\text{xx}}(\mathbf{k}, \omega)\} \approx \pi(1 + \cos \theta_{\mathbf{k}}) (g\mu_{\text{B}})^2 \frac{J_2(1 - |\gamma_{\mathbf{k}}|)}{\omega_{\mathbf{k}}^-} \delta(\omega - \omega_{\mathbf{k}}^-) + \pi(1 - \cos \theta_{\mathbf{k}}) (g\mu_{\text{B}})^2 \frac{J_2(1 + |\gamma_{\mathbf{k}}|)}{\omega_{\mathbf{k}}^+} \delta(\omega - \omega_{\mathbf{k}}^+), \quad (100)$$

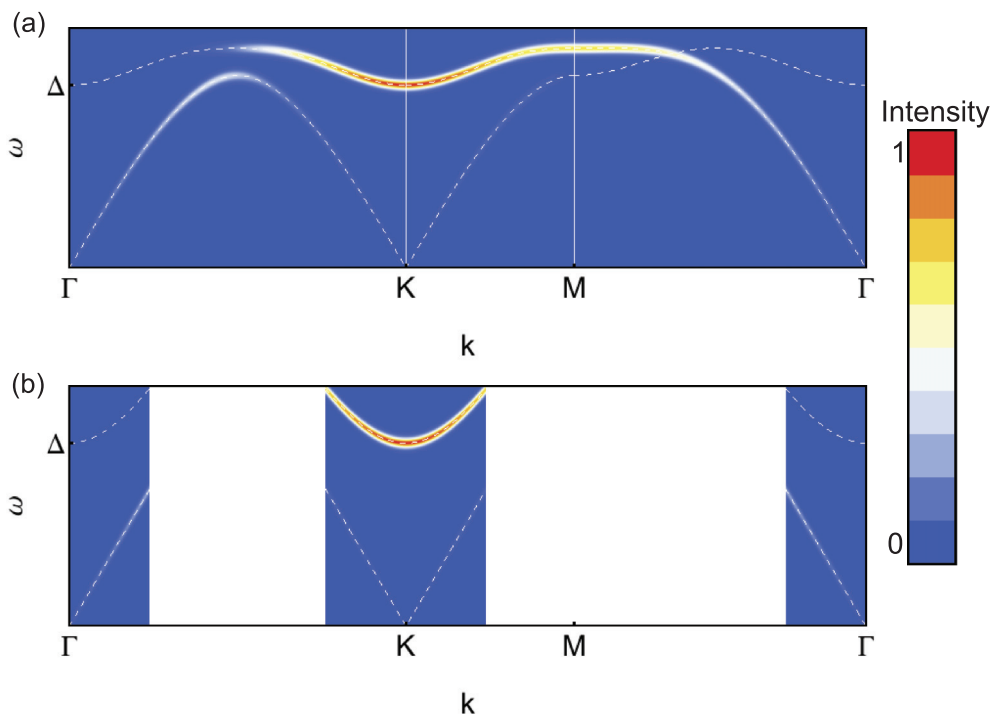


FIG. 12. (Color online) Prediction for inelastic neutron scattering from a state with three-sublattice antiferroquadrupolar (AFQ) spin nematic order of the type shown in Fig. 6. Animations showing the nature of the spin-dipole fluctuations associated with the gapless and gapped excitations are shown in Refs. 64 and 65, respectively. (a) Prediction of the microscopic flavor wave theory, as calculated from \mathcal{H}_{BBQ} [see Eq. (1)] for $J_1 = 1$, $J_2 = 1.22$ (cf. Refs. 40 and 41). The dashed white lines show the one-particle dispersion relations $\omega_{\mathbf{k}}^{\pm}$ [see Eq. (83)], where the gap to spin-wave excitations is $\Delta = 6\sqrt{J_2(J_2 - J_1)}$. (b) Prediction of the continuum theory $\mathcal{S}_{\Delta}^{\text{SU}(2)}[\phi]$ [see Eq. (80)] for the same set of parameters. The dashed white lines show the one-particle dispersion relations $\omega_{\mathbf{k}}^{\text{Q}}$ [see Eq. (81)] and $\omega_{\mathbf{k}}^{\text{S}}$ [see Eq. (82)]. The majority of the spectral weight is found in the spin-wave band, in the vicinity of the three-sublattice AFQ ordering vector $\mathbf{k}_K = (4\pi/3, 0)$. All predictions have been convoluted with a gaussian of FWHM 0.042Δ to mimic experimental resolution. The circuit Γ - K - M - Γ in reciprocal space is shown in Fig. 10.

where $\omega_{\mathbf{k}}^{\pm}$ is given in Eq. (83), $\gamma_{\mathbf{k}}$ in Eq. (61) and,

$$e^{i\theta_{\mathbf{q}}} = \frac{\gamma_{\mathbf{k}}}{|\gamma_{\mathbf{k}}|}. \quad (101)$$

Matching this to the predictions of the field theory for $\mathbf{k} \approx \mathbf{k}_K$, and translating parameters using Table I, we find exact, quantitative, agreement between the two approaches at long wavelength. This comparison is illustrated in Fig. 12.

3. Single-particle scattering near $\mathbf{k} = 0$

Close to the Γ point, we find a one-particle contribution to the dynamical susceptibility

$$\Im m\{\chi_{\text{S}}^{\text{xx}}(\mathbf{q}, \omega)\} \approx \frac{\pi}{2}(g\mu_{\text{B}})^2 \chi_{\perp}^{\text{Q}} \omega_{\mathbf{q}}^{\text{Q}} \delta(\omega - \omega_{\mathbf{q}}^{\text{Q}}), \quad (102)$$

where $\omega_{\mathbf{q}}^{\text{Q}}$ is given by Eq. (81) and $\mathbf{q} \approx 0$. This corresponds to a linearly dispersing quadrupole wave, whose intensity vanishes linearly for $\mathbf{q} \rightarrow 0$, but with four times the prefactor for scattering near \mathbf{k}_K . Once again this result is in quantitative agreement with the predictions of the lattice model \mathcal{H}_{BBQ} [see Eq. (1)].

While spin-wave excitations are defined for all \mathbf{k} , they do not contribute to single-particle scattering in the vicinity of the Γ point. This is because the dipole fluctuations on neighboring sublattices are exactly in antiphase, and therefore

cancel for $\mathbf{k} \rightarrow 0$. This cancellation is not accidental, but required by the $\text{SU}(2)$ symmetry of the spin-nematic state, and is a manifestation of the sum rule, Eq. (97).

4. Adding it all up

Figure 12 shows the result of summing all the 1-particle contributions to the $T = 0$ dynamic susceptibility, to give an overall prediction for inelastic neutron scattering from a three-sublattice AFQ state. Most of the spectral weight resides close to the K and K' points, in the spin-wave band. In contrast, quadrupole-waves contribute very little to scattering.

IV. DYNAMICAL QUADRUPOLAR SUSCEPTIBILITY

It is possible that a resonant technique, such as resonant x-ray scattering, could directly probe the 4-spin correlation function. This would provide access to the dynamical quadrupolar susceptibility. In the f -electron system UPd_3 , resonant x-ray scattering has been used to access the quadrupolar order parameter.⁷⁷⁻⁷⁹ While this is a different type of quadrupolar order, formed from a combination of spin and orbital degrees of freedom, the idea may carry over to the pure spin quadrupole considered in this publication. We therefore present predictions for $\Im m\{\chi_{\text{Q}}^{\alpha\beta\gamma\delta}(\mathbf{k}, \omega)\}$.

A. Quadrupolar excitations in a three-sublattice AFQ state

It follows from Eq. (93) [see Sec. II G] that, to linear order in ϕ ,

$$\delta\mathbf{Q}(\mathbf{r},t) \approx -\frac{2}{3} \begin{pmatrix} 0 \\ 0 \\ [(1 - e^{i\frac{2\pi}{3}})e^{i\mathbf{k}_K \cdot \mathbf{r}} + (1 - e^{-i\frac{2\pi}{3}})e^{-i\mathbf{k}_K \cdot \mathbf{r}}] \phi_1 \\ (e^{i\frac{2\pi}{3}} - e^{-i\frac{2\pi}{3}})(e^{i\mathbf{k}_K \cdot \mathbf{r}} - e^{-i\mathbf{k}_K \cdot \mathbf{r}}) \phi_3 \\ [(1 - e^{-i\frac{2\pi}{3}})e^{i\mathbf{k}_K \cdot \mathbf{r}} + (1 - e^{i\frac{2\pi}{3}})e^{-i\mathbf{k}_K \cdot \mathbf{r}}] \phi_2 \end{pmatrix} - \frac{\chi_{\perp}^S}{2} \begin{pmatrix} 0 \\ 0 \\ [2 + (1 + e^{i\frac{2\pi}{3}})e^{i\mathbf{k}_K \cdot \mathbf{r}} + (1 + e^{-i\frac{2\pi}{3}})e^{-i\mathbf{k}_K \cdot \mathbf{r}}] \partial_t \phi_4 \\ (2 - e^{i\mathbf{k}_K \cdot \mathbf{r}} - e^{-i\mathbf{k}_K \cdot \mathbf{r}}) \partial_t \phi_6 \\ -[2 + (1 + e^{-i\frac{2\pi}{3}})e^{i\mathbf{k}_K \cdot \mathbf{r}} + (1 + e^{i\frac{2\pi}{3}})e^{-i\mathbf{k}_K \cdot \mathbf{r}}] \partial_t \phi_5 \end{pmatrix}. \quad (103)$$

In this basis and at leading order in the perturbation expansion, the only nonzero entries in the susceptibility tensor are

$$\Im m\{\chi_Q^{xyxy}(\mathbf{k},\omega)\} = \Im m\{\chi_Q^{yzyz}(\mathbf{k},\omega)\} = \Im m\{\chi_Q^{zxzx}(\mathbf{k},\omega)\}, \quad (104)$$

and those related by the symmetry of the $Q^{\alpha\beta}$ tensor.

From Eq. (103), we can see that the ϕ_1 , ϕ_2 , and ϕ_3 Goldstone mode fields give a diverging contribution to the quadrupolar susceptibility approaching the Bragg peak at $\mathbf{k} = \mathbf{k}_K$. Conversely, the quadrupole fluctuations induced dynamically by the gapped, spin-wave modes are small as $\chi_{\perp}^S \partial_t \phi \sim \omega_{\mathbf{q}}^S$.

1. Single-particle scattering near to $\mathbf{k} = \mathbf{k}_K$

The dynamical quadrupolar susceptibility can be determined in an analogous manner to the spin susceptibility [see Sec. III C]. Close to $\mathbf{k} = \mathbf{k}_K$ the field theory predicts

$$\begin{aligned} \Im m\{\chi_Q^{xyxy}(\mathbf{k}_K + \mathbf{q},\omega)\} &\approx \frac{2\pi}{3} (g\mu_B)^4 \frac{1}{\chi_{\perp}^Q \omega_{\mathbf{q}}^Q} \delta(\omega - \omega_{\mathbf{q}}^Q) \\ &+ \frac{\pi}{8} (g\mu_B)^4 \chi_{\perp}^S \omega_{\mathbf{q}}^S \delta(\omega - \omega_{\mathbf{q}}^S), \end{aligned} \quad (105)$$

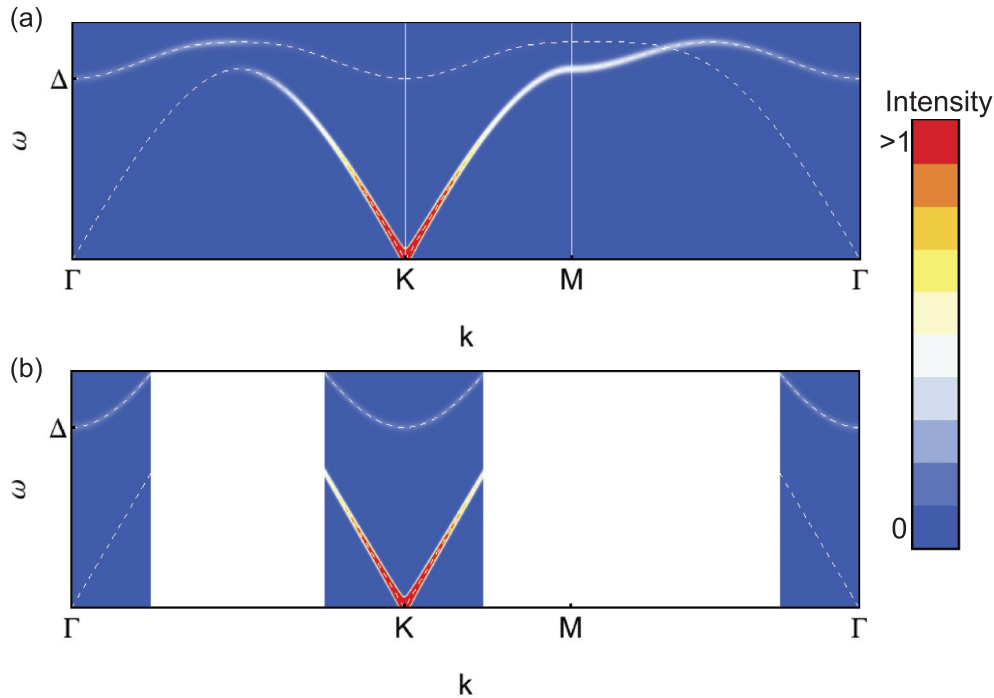


FIG. 13. (Color online) Prediction for the dynamical quadrupolar susceptibility, $\Im m\{\chi_Q^{xyxy}(\mathbf{k},\omega)\}$, for a state with three-sublattice antiferroquadrupolar (AFQ) spin nematic order of the type shown in Fig. 6. Animations showing the nature of the spin-dipole fluctuations associated with the gapless and gapped excitations are shown in Refs. 64 and 65, respectively. (a) Prediction of the microscopic flavor wave theory, as calculated from \mathcal{H}_{BBQ} [see Eq. (1)] for $J_1 = 1$, $J_2 = 1.22$. The dashed white lines show the one-particle dispersion relations $\omega_{\mathbf{k}}^{\pm}$ [see Eq. (83)], where the gap to spin-wave excitations is $\Delta = 6\sqrt{J_2(J_2 - J_1)}$. (b) prediction of the continuum theory $\mathcal{S}_{\Delta}^{\text{SU}(2)}[\phi]$ [see Eq. (80)] for the same set of parameters. The dashed white lines show the one-particle dispersion relations $\omega_{\mathbf{k}}^Q$ [see Eq. (81)] and $\omega_{\mathbf{k}}^S$ [see Eq. (82)]. The dominant feature is a diverging “Bragg peak” associated with the gapless, quadrupole-wave mode in the vicinity of the three-sublattice AFQ ordering vector $\mathbf{k}_K = (4\pi/3, 0)$. All predictions have been convoluted with a gaussian of FWHM 0.042Δ to mimic experimental resolution. The circuit Γ - K - M - Γ in reciprocal space is shown in Fig. 10.

where $\mathbf{q} \approx 0$. Scattering close to the K' point is exactly equivalent. Equation (105) shows that the intensity of scattering due to the quadrupolar modes diverges as $1/(\chi_{\perp}^Q \omega_{\mathbf{q}}^Q) \sim 1/|\mathbf{q}|$ for $\mathbf{q} \rightarrow 0$. Thus there is a ‘‘Bragg peak’’ in the quadrupolar susceptibility, as one expects for quadrupolar order. The gapped spin-wave modes induce a small quadrupole fluctuation, and this gives only a weak contribution to the susceptibility.

Linear flavor wave theory for the spin-1 BBQ model on the triangular lattice, \mathcal{H}_{BBQ} [see Eq. (1)], predicts

$$\begin{aligned} \Im m \{ \chi_{\text{Q}}^{\text{xyxy}}(\mathbf{k}, \omega) \} \\ \approx \pi(1 - \cos \theta_{\mathbf{k}})(g\mu_{\text{B}})^4 \frac{J_2(1 - |\gamma_{\mathbf{k}}|) + 2J_1|\gamma_{\mathbf{k}}|}{\omega_{\mathbf{k}}^-} \delta(\omega - \omega_{\mathbf{k}}^-) \\ + \pi(1 + \cos \theta_{\mathbf{k}})(g\mu_{\text{B}})^4 \\ \times \frac{J_2(1 + |\gamma_{\mathbf{k}}|) - 2J_1|\gamma_{\mathbf{k}}|}{\omega_{\mathbf{k}}^+} \delta(\omega - \omega_{\mathbf{k}}^+), \end{aligned} \quad (106)$$

and this is quantitative agreement with the field theory, Eq. (105), approaching the high-symmetry points.

2. Single-particle scattering near $\mathbf{k} = 0$

Close to the Γ point, we find a one-particle contribution to the dynamical quadrupolar susceptibility

$$\Im m \{ \chi_{\text{Q}}^{\text{xyxy}}(\mathbf{q}, \omega) \} \approx \frac{\pi}{2} (g\mu_{\text{B}})^4 \chi_{\perp}^{\text{S}} \omega_{\mathbf{q}}^{\text{S}} \delta(\omega - \omega_{\mathbf{q}}^{\text{S}}). \quad (107)$$

The quadrupole fluctuations induced dynamically by the gapped, spin-wave modes are suppressed by a factor $\chi_{\perp}^{\text{S}} \omega_{\mathbf{q}}^{\text{S}}$ and have low intensity compared to the diverging Goldstone mode at the K point. One interesting feature is that the gapless quadrupole mode at the Γ point does not appear in the field theory calculation of the susceptibility, due to the fact that neighboring quadrupoles beat in antiphase [see Eq. (93)]. This is in agreement with the flavor wave theory, Eq. (106), where the susceptibility turns on very slowly as $\Im m \{ \chi_{\text{Q}}^{\text{xyxy}}(\mathbf{q}, \omega) \} \sim q^5$.

3. Adding it all up

Figure 13 shows the result of summing all the 1-particle contributions to the $T = 0$ dynamic quadrupolar susceptibility, to give an overall prediction for scattering from a three-sublattice AFQ state. The dominant feature is the presence of ‘‘Bragg peaks’’ at the K and K' points. There is also a faint band where the gapped, spin-wave excitations dynamically induce a small, fluctuating quadrupole moment.

V. DISCUSSION AND CONCLUSIONS

Spin-nematic order remains an enigma. First proposed almost 40 years ago, and now studied in a wide range of theoretical models, it has never yet been unambiguously observed in experiment. Much of the difficulty in identifying a spin-nematic state arises from the fact that spin-nematic order does not break time-reversal symmetry. As a consequence, it cannot give rise to the internal magnetic fields measured by the common probes of static magnetic order—neutron scattering,

NMR, and muon spin rotation. In this respect, spin-nematic order has much in common with multipolar hidden-order phases in rare-earth magnets.⁵⁸ In principle, spin nematic order *could* be probed through its excitations. However, because of the complexity of the problem, these remain relatively poorly understood.

In this paper, we have attempted to narrow the gap between theory and experiment, by constructing a continuum field theory of a three-sublattice antiferroquadrupolar (AFQ) spin-nematic state. This field theory offers a ‘‘model-independent’’ approach to interpreting experiment, and can be used to explore the physical nature of the magnetic excitations of AFQ states. In the absence of magnetic field, we find that the long-wavelength excitations of AFQ states naturally divide into a set of three gapless, quadrupole-wave modes—the Goldstone modes—together with three gapped excitations with a strong spin-dipole character.

This field theory can also be used to make concrete predictions for the fluctuating spin-dipole fields associated with each type of excitation, and its associated signature in experiment. In this paper, we have focused on the most direct probe of spin-dipole fluctuations—inelastic neutron scattering. We find that quadrupole waves couple only weakly with neutrons, with the intensity of scattering vanishing linearly at low energies. However, the gapped modes possess a substantial dipole moment and couple strongly to neutrons. The observation of this gapped excitation, together with a set of ghostly low-energy Goldstone modes, in the *absence* of magnetic Bragg peaks, would constitute strong evidence for AFQ spin-nematic order.

Finally, we make predictions for the dynamical quadrupole susceptibility. This exhibits diverging Bragg-peak like intensity approaching the Goldstone modes, along with a very faint gapped mode. As in the f -electron systems, this may be measurable using resonant x-ray scattering. Such experiments would directly probe the order parameter, and could in consequence provide compelling evidence for the existence of spin-nematic order. How these excitations evolve with field, and what their consequences are for NMR $1/T_1$ relaxation rates will be explored in separate publications.^{63,80,81}

An obvious question for future work is the role of interactions. As in the case of FQ order,⁶² interactions between the Goldstone modes of the AFQ state endow these excitations with a finite, k^2 -dependent lifetime. There is also a corresponding renormalization of the director stiffness, $\rho_{\text{d}}^{\text{Q}}$, leading to small changes in the velocity of the Goldstone modes. However, the most interesting features come from the interaction between the Goldstone modes and the gapped, long-wavelength ‘‘spin-wave’’ modes. This is true both from an experimental point of view, since the gapped modes support large spin-dipole fluctuations, and a theoretical point of view, where these type of interactions have not been as thoroughly explored as those between Goldstone modes. We will return to these effects in a future paper.⁶³

In conclusion, the SU(3) generalization of the nonlinear σ model developed in this text provides a robust means of characterising spin-nematic states with antiferroquadrupolar order, which is independent of any particular microscopic model. This σ model approach provides an excellent starting point for understanding the universal behavior of spin-nematic states

and leads to concrete, testable predictions for experiment. For this reason, it can serve as an important tool for establishing whether spin-nematic order exists in a wide variety of real materials. We hope that the waves predicted by the σ model will, in the near future, be seen.

ACKNOWLEDGMENTS

We are grateful to Tsutomu Momoi for a number helpful comments on this work and to Karlo Penc for a careful reading of the manuscript. This research was supported under EPSRC grants EP/C539974/1 and EP/G031460/1

-
- ¹P. A. Lee, *Science* **321**, 1306 (2008).
²M. Blume and Y. Hsieh, *J. Appl. Phys.* **40**, 1249 (1969).
³H. Chen and P. Levy, *Phys. Rev. Lett.* **27**, 1383 (1971).
⁴A. F. Andreev and I. A. Grishchuk, *Zh. Eksp. Teor. Fiz.* **87**, 467 (1984) [*Sov. Phys. JETP* **60**, 267 (1984)].
⁵N. Papanicolaou, *Nucl. Phys. B* **305**, 367 (1988).
⁶P. Chandra and P. Coleman, *Phys. Rev. Lett.* **66**, 100 (1991).
⁷V. Barzykin, L. P. Gorkov, and A. Sokol, *Europhys. Lett.* **15**, 869 (1991).
⁸V. Barzykin and L. P. Gorkov, *Phys. Rev. Lett.* **70**, 2479 (1993).
⁹K. Penc and A. Lauchli, *Introduction to Frustrated Magnetism* (Springer-Verlag, Berlin, Heidelberg, 2011), Chap. 13.
¹⁰A. V. Chubukov, *J. Phys.: Condens. Matter* **2**, 4455 (1990).
¹¹A. V. Chubukov, *Phys. Rev. B* **44**, 4693 (1991).
¹²R. O. Kuzian and S.-L. Drechsler, *Phys. Rev. B* **75**, 024401 (2007).
¹³T. Vekua, A. Honecker, H. J. Mikeska, and F. Heidrich-Meisner, *Phys. Rev. B* **76**, 174420 (2007).
¹⁴L. Kecke, T. Momoi, and A. Furusaki, *Phys. Rev. B* **76**, 060407 (2007).
¹⁵T. Hikihara, L. Kecke, T. Momoi, and A. Furusaki, *Phys. Rev. B* **78**, 144404 (2008).
¹⁶J. Sudan, A. Luscher, and A. M. Lauchli, *Phys. Rev. B* **80**, 140402 (2009).
¹⁷S. Nishimoto, S.-L. Drechsler, R. Kuzian, J. Richter, and J. van den Brink, *J. Phys.: Conf. Ser.* **400**, 032069 (2012).
¹⁸D. C. Cabra, A. Honecker, and P. Pujol, *Eur. Phys. J. B* **13**, 55–73 (2000).
¹⁹A. V. Chubukov, *J. Phys. C* **20**, L509 (1987).
²⁰A. V. Chubukov, *J. Phys.: Condens. Matter* **3**, 2665 (1991).
²¹A. V. Syromyatnikov, *Phys. Rev. B* **86**, 014423 (2012).
²²F. Heidrich-Meisner, A. Honecker, and T. Vekua, *Phys. Rev. B* **74**, 020403(R) (2006).
²³H. T. Lu, Y. J. Wang, Shaojin Qin, and T. Xiang, *Phys. Rev. B* **74**, 134425 (2006).
²⁴A. A. Nersesyan, A. O. Gogolin, and F. H. L. Essler, *Phys. Rev. Lett.* **81**, 910 (1998).
²⁵K. Totsuka, P. Lecheminant, and S. Capponi, *Phys. Rev. B* **86**, 014435 (2012).
²⁶A. Lauchli, G. Schmid, and S. Trebst, *Phys. Rev. B* **74**, 144426 (2006).
²⁷S. R. Manmana, A. M. Lauchli, F. H. L. Essler, and F. Mila, *Phys. Rev. B* **83**, 184433 (2011).
²⁸G. Fath and J. Solyom, *Phys. Rev. B* **51**, 3620 (1995).
²⁹N. Shannon, T. Momoi, and P. Sindzingre, *Phys. Rev. Lett.* **96**, 027213 (2006).
³⁰R. Shindou and T. Momoi, *Phys. Rev. B* **80**, 064410 (2009).
³¹H. T. Ueda and K. Totsuka, *Phys. Rev. B* **80**, 014417 (2009).
³²R. Shindou, S. Yunoki, and T. Momoi, *Phys. Rev. B* **84**, 134414 (2011).
³³R. Shindou, S. Yunoki, and T. Momoi, *Phys. Rev. B* **87**, 054429 (2013).
³⁴T. Momoi, P. Sindzingre, and N. Shannon, *Phys. Rev. Lett.* **97**, 257204 (2006).
³⁵T. Momoi, P. Sindzingre, and K. Kubo, *Phys. Rev. Lett.* **108**, 057206 (2012).
³⁶A. Läuchli, J. C. Domenge, C. Lhuillier, P. Sindzingre, and M. Troyer, *Phys. Rev. Lett.* **95**, 137206 (2005).
³⁷F. P. Onufrieva, *Zh. Eksp. Teor. Fiz.* **89**, 2270 (1985) [*Sov. Phys. JETP* **62**, 1311 (1985)].
³⁸A. Joshi, M. Ma, F. Mila, D. N. Shi, and F. C. Zhang, *Phys. Rev. B* **60**, 6584 (1999).
³⁹A. Lauchli, F. Mila, and K. Penc, *Phys. Rev. Lett.* **97**, 087205 (2006).
⁴⁰H. Tsunetsugu and M. Arikawa, *J. Phys. Soc. Jpn.* **75**, 083701 (2006).
⁴¹H. Tsunetsugu and M. Arikawa, *J. Phys.: Condens. Matter* **19**, 145248 (2007).
⁴²T. A. Toth, A. M. Lauchli, F. Mila, and K. Penc, *Phys. Rev. Lett.* **105**, 265301 (2010).
⁴³T. A. Toth, A. M. Lauchli, F. Mila, and K. Penc, *Phys. Rev. B* **85**, 140403 (2012).
⁴⁴R. K. Kaul, *Phys. Rev. B* **86**, 104411 (2012).
⁴⁵K. Harada and N. Kawashima, *Phys. Rev. B* **65**, 052403 (2002).
⁴⁶M. E. Zhitomirsky, *Phys. Rev. B* **78**, 094423 (2008).
⁴⁷J. T. Chalker, P. C. W. Holdsworth, and E. F. Shender, *Phys. Rev. Lett.* **68**, 855 (1992).
⁴⁸R. Moessner and J. T. Chalker, *Phys. Rev. Lett.* **80**, 2929 (1998).
⁴⁹R. Moessner and J. T. Chalker, *Phys. Rev. B* **58**, 12049 (1998).
⁵⁰N. Shannon, K. Penc, and Y. Motome, *Phys. Rev. B* **81**, 184409 (2010).
⁵¹J. M. Hopkinson, S. V. Isakov, H.-Y. Kee, and Y. B. Kim, *Phys. Rev. Lett.* **99**, 037201 (2007).
⁵²M. Sato, T. Hikihara, and T. Momoi, *Phys. Rev. Lett.* **110**, 077206 (2013).
⁵³S. Nakatsuji, Y. Nambu, H. Tonomura, O. Sakai, S. Jonas, C. Broholm, H. Tsunetsugu, T. Qiu, and Y. Maeno, *Science* **309**, 1697 (2005).
⁵⁴S. Bhattacharjee, V. B. Shenoy, and T. Senthil, *Phys. Rev. B* **74**, 092406 (2006).
⁵⁵E. M. Stoudenmire, S. Trebst, and L. Balents, *Phys. Rev. B* **79**, 214436 (2009).
⁵⁶L. E. Svistov *et al.*, *JETP Lett.* **93**, 21 (2010).
⁵⁷M. E. Zhitomirsky and H. Tsunetsugu, *Europhys. Lett.* **92**, 37001 (2010).
⁵⁸P. Santini, S. Carretta, and G. Amoretti, *Rev. Mod. Phys.* **81**, 807 (2009).
⁵⁹B. A. Ivanov and A. K. Kolezhuk, *Phys. Rev. B* **68**, 052401 (2003).
⁶⁰B. A. Ivanov and R. S. Khymyn, *JETP* **104**, 307 (2007).

- ⁶¹B. A. Ivanov, R. S. Khymyn, and A. K. Kolezhuk, *Phys. Rev. Lett.* **100**, 047203 (2008).
- ⁶²V. G. Bar'yakhtar, V. I. Butrim, A. K. Kolezhuk, and B. A. Ivanov, *Phys. Rev. B* **87**, 224407 (2013).
- ⁶³A. Smerald and N. Shannon (unpublished).
- ⁶⁴See Supplemental Material at <http://link.aps.org/supplemental/10.1103/PhysRevB.88.184430> for animation showing the nature of the quadrupole-wave modes, calculated directly from the linearized continuum field theory $\mathcal{S}_{\Delta}^{\text{SU}(2)}[\phi]$ [see Eq. (80)]. The animation shows an equally weighted superposition of the fields ϕ_1 , ϕ_2 and ϕ_3 . A large, coherent fluctuation in the \mathbf{u} field [see Eq. (14)], and therefore the quadrupole moments, is accompanied by a small, dynamically generated spin-dipole fluctuation. The red line shows the motion of \mathbf{u} , the black arrow that of the spin dipole \mathbf{S} [see Eq. (13)], and the blue surface gives the probability distribution for the direction of the spin within the coherent state representation. The motion is shown for $\mathbf{q} = (0.1, 0.1)$ and for parameters $J_1 = 1$ and $J_2 = 1.22$.
- ⁶⁵See Supplemental Material at <http://link.aps.org/supplemental/10.1103/PhysRevB.88.184430> for animation showing the nature of the spin-wave modes, calculated directly from the linearized continuum field theory. A large, coherent fluctuation in the spin-dipole field, is accompanied by a small, dynamically generated quadrupole fluctuation. The animation shows an equally weighted superposition of the fields ϕ_4 , ϕ_5 , and ϕ_6 . (See Ref. 64 for further details.)
- ⁶⁶B. Bauer, P. Corboz, A. M. Lauchli, L. Messio, K. Penc, M. Troyer, and F. Mila, *Phys. Rev. B* **85**, 125116 (2012).
- ⁶⁷N. Papanicolaou, *Nucl. Phys. B* **240**, 281 (1984).
- ⁶⁸P. Li, G. M. Zhang, and S. Q. Shen, *Phys. Rev. B* **75**, 104420 (2007).
- ⁶⁹V. I. Butrim, B. A. Ivanov, A. S. Kuznetsov, and R. S. Khymyn, *Fiz. Nizk. Temp.* **34**, 1266 (2008) [*Low Temp. Phys.* **34**, 997 (2008)].
- ⁷⁰T. Dombre and N. Read, *Phys. Rev. B* **39**, 6797 (1989).
- ⁷¹W. Apel, M. Wintel, and H. U. Everts, *Z. Phys. B* **86**, 139 (1992).
- ⁷²E. Fradkin, *Field Theories of Condensed Matter Systems* (Cambridge University Press, 2013).
- ⁷³A. Auerbach, *Interacting Electrons and Quantum Magnetism* (Springer-Verlag, New York, 1994).
- ⁷⁴S. Chakravarty, B. I. Halperin, and D. R. Nelson, *Phys. Rev. B* **39**, 2344 (1989).
- ⁷⁵S. Allen and D. Loss, *Physica A* **239**, 47 (1997).
- ⁷⁶P. Azaria, B. Delamotte, F. Delduc, and T. Jolicoeur, *Nucl. Phys. B* **408**, 485 (1993).
- ⁷⁷D. F. McMorrow, K. A. McEwen, U. Steigenberger, H. M. Ronnow, and F. Yakhov, *Phys. Rev. Lett.* **87**, 057201 (2001).
- ⁷⁸H. C. Walker, K. A. McEwen, D. F. McMorrow, S. B. Wilkins, F. Wastin, E. Colineau, and D. Fort, *Phys. Rev. Lett.* **97**, 137203 (2006).
- ⁷⁹H. C. Walker, K. A. McEwen, M. D. Le, L. Paolasini, and D. Fort, *J. Phys.: Condens. Matter* **20**, 395221 (2008).
- ⁸⁰A. Smerald and N. Shannon, *Phys. Rev. B* **84**, 184437 (2011).
- ⁸¹A. Smerald and N. Shannon, arXiv:1303.4465.